

## SELF-SIMILAR COLLAPSE OF ROTATING MAGNETIC MOLECULAR CLOUD CORES

RUBEN KRASNOPOLSKY AND ARIEH KÖNIGL<sup>1</sup>

Department of Astronomy and Astrophysics, University of Chicago, 5640 South Ellis Avenue, Chicago, IL 60637  
{ruben,arieh}@oddjob.uchicago.edu

Submitted 2002 May 1; accepted 2002 August 5

### ABSTRACT

We present self-similar solutions that describe the gravitational collapse of rotating, isothermal, magnetic molecular-cloud cores. These solutions make it possible, for the first time, to study the formation of rotationally supported protostellar disks of the type detected around many young stellar objects in the context of a realistic scenario of star formation in magnetically supported, weakly ionized, molecular cloud cores. This work focuses on the evolution after a point mass first forms at the center and generalizes previous results by Contopoulos, Ciolek, & Königl that did not include rotation. Our semianalytic scheme incorporates ambipolar diffusion and magnetic braking and allows us to examine the full range of expected behaviors and their dependence on the physical parameters. We find that, for typical parameter values, the inflow first passes through an ambipolar-diffusion shock (at a radius  $r_a$ ), where the magnetic flux decouples from the matter, and subsequently through a centrifugal shock (at  $r_c$ ), inward of which a rotationally supported disk (of mass  $M_d$ ) is established. By the time ( $\sim 10^5$  yr) that the central mass  $M_c$  grows to  $\sim 1 M_\odot$ ,  $r_a \gtrsim 10^3$  AU,  $r_c \gtrsim 10^2$  AU, and  $M_d/M_c \lesssim 0.1$ . The derived disk properties are consistent with data on T Tauri systems, and our results imply that protostellar disks may well be Keplerian also during earlier phases of their evolution. We demonstrate that the disk is likely to drive centrifugal outflows that transport angular momentum and mass, and we show how the radially self-similar wind solution of Blandford & Payne can be naturally incorporated into the disk model. We further verify that gravitational torques and magnetorotational instability-induced turbulence typically do not play an important role in the angular momentum transport. For completeness, we also present solutions for the limiting cases of fast rotation (where the collapse results in a massive disk with such a large outer radius that it traps the ambipolar-diffusion front) and strong braking (where no disk is formed and the collapse resembles that of a nonrotating core at small radii), as well as solutions describing the rotational collapse of ideal-MHD and of nonmagnetic model cores.

*Subject headings:* accretion, accretion disks — diffusion — ISM: clouds — ISM: magnetic fields — MHD — shock waves — stars: formation

### 1. INTRODUCTION

Low-mass star formation is believed to occur predominantly in molecular cloud cores. The commonly accepted scenario is that dense molecular clouds are supported against self-gravity by magnetic and thermal stresses. Since the gas is only weakly ionized, the clouds are not in a strict steady state: the prevalent neutral molecules, pulled in by the force of gravity, gradually drift inward through the magnetic field (attached to the ionized component and anchored in the cloud envelope) in a process known as ambipolar diffusion. When the mass-to-flux ratio in the cloud core exceeds a critical value, the core undergoes gravitational collapse to form a central protostar. The core evolution after the collapse is initiated can in general be divided into two phases: a rapid initial dynamical contraction, which proceeds nonhomologously and eventually results in the formation of a central point mass, followed by an accretion phase, during which the central mass gradually increases and its gravitational field dominates a progressively larger region around the origin. The evolution of star-forming molecular clouds has been studied mostly through numerical simulations (see, e.g., Mouschovias & Ciolek 1999 for a review). Until recently, these calculations were terminated before the end of the dynamical-collapse phase, basically at the point where radiative trapping near the center started to invalidate the isothermality assumption adopted in these computations. However, Ciolek & Königl (1998, hereafter CK) circumvented this problem by treating the comparatively small region of radiative trapping as a central

sink cell; this enabled them to model the collapse of nonrotating magnetic cloud cores through point-mass formation (PMF) and into the protostellar accretion phase. Concurrently, Contopoulos, Ciolek, & Königl (1998, hereafter CCK) obtained semi-analytic self-similar solutions that explicitly accounted for the effects of ambipolar diffusion and successfully reproduced the main qualitative features of the numerical simulations of CK.

Our goal in this paper is to extend the previous work on the post-PMF evolution of collapsing magnetic cloud cores by including the effects of rotation. Molecular line observations (e.g., Goodman et al. 1993; Kane & Clemens 1997) have established that a majority of dense ( $\gtrsim 10^4 \text{ cm}^{-3}$ ) cloud cores show evidence of rotation, with angular velocities  $\sim 3 \times 10^{-15} - 10^{-13} \text{ s}^{-1}$  that tend to be uniform on scales of  $\sim 0.1 \text{ pc}$ , and with specific angular momenta in the range  $\sim 4 \times 10^{20} - 3 \times 10^{22} \text{ cm}^2 \text{ s}^{-1}$ . Although present, the rotation contributes only a small fraction (typically no more than a few percent) to the dynamical support of these cores, and self-gravity is mostly balanced by magnetic and thermal stresses. During their quasistatic contraction phase, the cores evidently lose angular momentum by means of magnetic braking — the magnetic transfer of angular momentum to the ambient gas through torsional Alfvén waves — and this process also tends to align their angular velocity and large-scale magnetic field vectors (e.g., Mouschovias & Ciolek 1999). Once dynamical collapse is initiated and a core goes into a near-free-fall state, the specific angular momentum is expected to be approximately conserved,

<sup>1</sup> Also at the Enrico Fermi Institute, University of Chicago.

resulting in a progressive increase in the centrifugal force that eventually halts the collapse and gives rise to a rotationally supported disk. These expectations are consistent with the results of molecular-line interferometric observations, which have probed contracting cloud cores on scales  $\sim 10^2\text{--}10^3$  AU (e.g., Myers, Evans, & Ohashi 2000; Mundy, Looney, & Welch 2000; Wilner & Lay 2000). These observations have revealed that, on scales  $\lesssim 10^3$  AU, the cores have a flattened, thick-disk morphology and a velocity field that is dominated by infall motions (with only a modest rotational component). This morphology is consistent with numerical simulations of magnetically supported clouds, which have demonstrated that the gas rapidly contracts along the field lines and maintains force equilibrium along the field even during the collapse phase (e.g., Fiedler & Mouschovias 1993; Galli & Shu 1993; CK), including in cases where the clouds are initially elongated in the field direction (e.g., Nakamura, Hanawa, & Nakano 1995; Tomisaka 1996). The observations have also established that angular momentum is by and large conserved in the infalling gas (e.g., Ohashi et al. 1997) and leads to the formation of rotationally supported disks on scales  $\lesssim 10^2$  AU.

The pre-PMF collapse of rotating, magnetized, weakly ionized cloud cores was previously studied by Basu & Mouschovias (1994, 1995a,b). They found that little angular momentum is lost during the dynamical-collapse phase but that the centrifugal force nevertheless does not become important prior to PMF. In the current work we focus on the post-PMF phase of the collapse, which enables us to model the formation of circumstellar disks in the context of magnetic cloud cores and to study their properties and their role in the buildup of the central protostar. Circumstellar disks have been detected in  $\sim 25\text{--}50\%$  of pre-main-sequence stars in nearby dark clouds (e.g., Beckwith & Sargent 1993), and it is likely that most of the mass assembled in a typical low-mass young stellar object (YSO) is accreted through a disk (e.g., Calvet, Hartmann, & Strom 2000). The study of protostellar disks is important also because they are the incubators of planetary systems, so their properties are directly relevant to the process of planet formation (e.g., Wuchterl, Guillot, & Lissauer 2000). The rotational properties of the collapsing core are evidently also of particular relevance to the question of multiple-star formation (e.g., Bodenheimer et al. 2000). In the ensuing discussion we assume that the collapsing core does not give rise to more than one stellar object; we nevertheless briefly address the issue of core fragmentation in § 4.

The studies of CK and CCK demonstrated that ambipolar diffusion, which is unimportant during the dynamical pre-PMF collapse phase, is “revitalized” after a point mass starts to grow in the center and leads to a decoupling of the magnetic flux from the inflowing gas. It was found that the “decoupling front” propagates outward in the form of a hydromagnetic shock (as originally suggested by Li & McKee 1996) and that this process can go a long way toward resolving the magnetic flux problem in star formation (the several-orders-of-magnitude discrepancy between the empirical upper limit on the magnetic flux of a protostar and the flux associated with the corresponding mass in the pre-collapse core). By incorporating rotation into the picture, we can study how this issue is affected by the formation of a disk. Furthermore, as our model includes angular momentum transport (by the large-scale magnetic field), which is crucial for enabling mass to accumulate in the center and form a protostar (see § 2.1), we are also in a position to address the angular

momentum problem in star formation (analogous to the magnetic flux problem, except that the quantity under consideration is the specific angular momentum).

The emergence of a quasi-stationary, rotationally supported disk from a nearly freely falling, collapsing core inevitably involves a strong deceleration of the inflowing matter, which almost invariably takes place in a shock. This “centrifugal” shock is distinct from the ambipolar-diffusion shock mentioned above: it is typically hydrodynamic, rather than hydromagnetic, in nature, and it is generally located at a different distance from the center. The appearance of a second shock increases the complexity of the problem, and it might seem that it could only be tackled through a multi-scale numerical simulation. However, we have found that it is possible to treat this problem semianalytically by generalizing the self-similar solutions presented in CCK to include the effects of rotation and magnetic braking. Although this treatment is somewhat less detailed than a numerical simulation, the semianalytic approach allows us to more readily explore the fairly extensive parameter space. This approach is supported by the strong evidence from numerical simulations that a multiscale core collapse naturally leads to a self-similar evolution. In particular, this behavior has been found to describe the effectively magnetic flux- and angular momentum-conserving *pre*-PMF collapse phase of a rotating magnetic core seen in the aforementioned numerical simulations of Basu & Mouschovias (Basu 1997; Nakamura et al. 1999; see also Narita, Hayashi, & Miyama 1984 and Li & Shu 1997). As regards the post-PMF evolution, Saigo & Hanawa (1998) obtained similarity solutions for flattened cloud cores that approximate previous numerical simulations of the collapse of rotating clouds through the moment when a central point mass could be expected to form. The good correspondence between the CCK solutions and the nonrotating magnetic collapse simulations of CK further strengthens our confidence in the viability of this approach.

In relating this work to previously published results, we note that neither the Saigo & Hanawa (1998) model nor the numerical simulations with which they compare their solutions incorporate an angular momentum transport mechanism, and therefore they do not in practice give rise to a central point mass. (Nevertheless, as we discuss in § 3.1, their post-PMF solutions correspond to a limiting case of the more general model considered in this paper.) It is also worth mentioning in this connection that self-similar models of the gravitational collapse of rotating, disk-like mass distributions that incorporate *viscous* angular momentum transport have been constructed by Mineshige & Umemura (1997) and Tsuribe (1999). However, the former model arbitrarily imposes an inner boundary condition that does not allow mass to accumulate at the center, whereas the latter model is restricted to the case in which the inflow speed is everywhere so low that no centrifugal shock forms. Neither of these models therefore provides a realistic framework for studying star formation in rotating molecular cloud cores.

The plan of this paper is as follows. In § 2 we formulate the problem, discuss the adopted approximations, and describe the self-similar model. In § 3 we present illustrative solutions, ordered by increasing level of complexity, which isolate different aspects of the full problem. We use the flexibility afforded by our semianalytic approach to examine the dependence of the results on the efficiency of ambipolar diffusion and magnetic braking and to elucidate the interplay between these two processes. We give a general discussion of these solutions and of

their astrophysical implications in § 4, where we also consider the production of centrifugally driven disk outflows. Our conclusions are summarized in § 5.

## 2. SELF-SIMILAR MODEL

### 2.1. Formulation of the Problem

Our basic model setup is the same as in CCK. We consider an isothermal, disklike core that contracts in the radial direction while maintaining a vertical hydrostatic equilibrium at all times. As noted in § 1, this behavior was found in numerical simulations of isothermal cores that are initially supported against gravitational collapse by a large-scale, ordered magnetic field. Nonmagnetic simulations (e.g., Norman, Wilson, & Barton 1980; Narita, Hayashi, & Miyama 1984; Matsumoto, Hanawa, & Nakamura 1997) have established that rotation could further contribute to the tendency of a core to flatten as it contracts so long as the specific angular momentum is approximately conserved. In restricting gas motions in our model to the plane of the flattened core, we preclude the possibility that matter can reach the center from above (or below) the disk, and this, in turn, implies that a point mass can form in the center only if there exists a mechanism for removing angular momentum from the inflowing gas. There have also been models in which the complementary view has been adopted, viz., new mass is added to the protostar and its circumstellar disk only from above and below the disk plane (e.g., Terebey, Shu, & Cassen 1984; Yorke, Bodenheimer, & Laughlin 1993). These models tend to produce rotationally supported disks whose masses are comparable to that of the central star, even if angular momentum transport within the disk is taken into account (e.g., Cassen & Summers 1983; Lin & Pringle 1990). However, most observed protostellar disks in nearby dark clouds have masses (estimated from dust emission or, when possible, from a direct measurement of the disk velocity field) that are significantly smaller ( $\lesssim 10\%$ ) than the protostellar mass (e.g., Beckwith & Sargent 1993). As we demonstrate in § 3, such low-mass systems can form naturally when mass flows into the central region primarily in the disk plane. Given that this is the expected situation for magnetically regulated core contraction and that the disklike configurations predicted in this case are consistent with observations of collapsing cloud cores, we consider this approximation to be adequate for capturing the essence of protostellar-disk and star formation.

The isothermality assumption was justified in the work of CK and CCK on the grounds that it generally applies so long as the density remains below  $\sim 10^{10} \text{ cm}^{-3}$ , which for a typical nonrotating collapse is the case on scales  $\gtrsim 5 \text{ AU}$ . This assumption is less tenable in the present work because, when a quasi-stationary, centrifugally supported disk forms, it has a significantly higher column density at a given radius than a nearly freely falling configuration, with the result that radiative trapping already occurs on scales  $\lesssim 10^2 \text{ AU}$  (e.g., Wardle & Königl 1993). Irradiation by the central protostar tends to mitigate this effect and establish vertical isothermality in the outer regions of the disk, but, in turn, it leads to a moderately strong ( $T \propto r^{-1/2}$ ) variation of the disk temperature with radius (e.g., D'Alessio et al. 1998). However, since thermal stresses turn out not to play a major role in the core-collapse dynamics, the assumption of isothermality (which is required for self-similarity) is not likely to introduce significant inaccuracies into the results.

Another requirement for self-similarity is that the ion density

$\rho_i$  be proportional to the square root of the neutral mass density (which is essentially equal to the total gas density  $\rho$ ). In this case, the ratio  $\eta$  of the neutral-ion momentum-exchange time scale  $\tau_{ni}$  to the nominal self-gravity free-fall time  $(4\pi G\rho)^{-1/2}$  is independent of density and can be treated as a constant.<sup>2</sup> This behavior is found at comparatively low densities, when molecular ionization by cosmic rays (at a rate  $\xi = 10^{-17} \xi_{-17} \text{ s}^{-1}$ ) is balanced by rapid dissociative recombination of the molecular ions and the dominant positive charges are metal ions (formed by a charge-exchange reaction between molecular ions and neutral metal atoms and destroyed by recombination on grain surfaces). For grains of radius  $a = 0.1 \mu\text{m}$ , a temperature  $T = 10 \text{ K}$ , and  $\xi_{-17} \approx 1$ , this scaling applies roughly at neutral particle densities between  $\sim 10^4 \text{ cm}^{-3}$  and  $\lesssim 10^7 \text{ cm}^{-3}$  (e.g., Ciolek & Mouschovias 1998; Kamaya & Nishi 2000). These values of  $T$  and  $n$  characterize the outer regions of collapsing cores, typically on scales  $\gtrsim 10^3 \text{ AU}$  (e.g., CK). In this regime,  $\eta \approx 0.2 \xi_{-17}^{-1/2}$ .

The numerical models of CK extended to scales  $\lesssim 10 \text{ AU}$ , where densities  $\gtrsim 10^{10} \text{ cm}^{-3}$  were attained. In the case of a rotationally supported disk, even higher densities are expected on these scales. At such high densities, grains are typically the dominant carriers of both positive and negative charges, and their densities also scale as  $n^{1/2}$  (e.g., Nishi, Nakano, & Umebayashi 1991). Assuming, for the sake of illustration, that the charged grain distribution is dominated by a population of small (PAH-like) singly charged particles of radius  $a$  (see Neufeld & Hollenbach 1994), we can deduce the charged-grain number density  $n_{\pm}$  from the ionization balance relation

$$\xi n = \pi(2a)^2 n_{\pm}^2 \left( \frac{8kT}{\pi m_{\pm r}} \right)^{1/2} \left( 1 + \frac{e^2}{2akT} \right), \quad (1)$$

where  $m_{\pm r} = 2\pi a^3 \rho_s / 3$  (with  $\rho_s \approx 2.3 \text{ g cm}^{-3}$ ) is the reduced grain mass. Taking as fiducial values  $n = 10^{12} n_{12} \text{ cm}^{-3}$  and  $T = 10^2 T_2 \text{ K}$  at a distance  $r \approx 10 \text{ AU}$  from the center of a rotationally supported protostellar disk, we can neglect the factor 1 in comparison with the second term in the last parentheses on the right-hand side of equation (1) (which accounts for the electrostatic attraction between the recombining grains). We then get  $n_{\pm} \approx 15.8(a/5 \text{ \AA})^{1/4} T_2^{1/4} \xi_{-17}^{1/2} n_{12}^{1/2} \text{ cm}^{-3}$ . Assuming that the small grains are characterized by the same rate coefficient for momentum transfer through elastic scattering with neutrals as metal ions ( $\langle \sigma v \rangle_{\pm n} \approx 1.7 \times 10^{-9} \text{ cm}^3 \text{ s}^{-1}$ ; see Wardle & Ng 1999), we obtain  $\eta \approx 0.07 \xi_{-17}^{-1/2} T_2^{-1/4} (a/5 \text{ \AA})^{-1/4}$  in this density regime. Ambipolar diffusion will dominate Ohmic diffusivity so long as the grain Hall parameter  $\beta_{\pm}$  (the ratio of the cyclotron frequency to the collision frequency with neutrals) exceeds 1. Adopting a fiducial magnetic field strength at  $r = 10 \text{ AU}$  of  $B = 0.3 \text{ G}$ , we find  $\beta_{\pm} \approx 0.7(B/0.3 \text{ G})/n_{12}$ , which we expect to climb securely above 1 as the density continues to decrease with increasing  $r$ . We thus infer that both the low- and the high-density regimes of our model collapsing cores correspond to ambipolar diffusion that is amenable to self-similar scaling. The intermediate density regime will depart from this scaling (e.g., Nishi et al. 1991), and it is also likely to involve significant contributions from the Hall current term in Ohm's law (e.g., Wardle & Königl 1993; Wardle & Ng 1999). Nevertheless, given that our bracketing values of the parameter  $\eta$  vary by only one order of magnitude (assuming that  $\xi_{17}$  lies in

<sup>2</sup> Our dimensionless ambipolar diffusion parameter  $\eta \equiv \tau_{ni}(4\pi G\rho)^{1/2}$  is smaller than the one used in CCK by a factor  $\sqrt{2}$ .

the range  $\sim 1$ – $10$ ) across  $\sim 8$  orders of magnitude in density, we may expect our diffusivity parameterization to yield qualitatively meaningful results on all scales between  $\sim 10$  AU and  $\sim 10^4$  AU.

Just as in CCK, we take the initial ( $t = 0$ ) state of our model core to coincide with the endpoint of the pre-PMF collapse phase, which is characterized by a radial scaling of the surface density  $\Sigma$  and the vertical magnetic field component  $B_z \propto r^{-1}$  and by spatially constant radial inflow velocity  $V_r(t = 0) \equiv u_0 C$  (where  $C$  is the isothermal speed of sound) and mass accretion rate  $\dot{M}_0 \equiv -A(u_0 C^3/G)$ . In the presence of rotation, this state also exhibits a uniform azimuthal speed. Since the latter is typically much smaller than the speed of sound  $C \approx 0.19(T/10\text{K})^{1/2} \text{ km s}^{-1}$ , we normalize our initial state as in CCK based on the nonrotational collapse simulations of CK ( $u_0 \approx -1$  and  $A \approx 3$ ). We determine the initial value of  $V_\phi/C$  (which we denote by  $v_0$ ) from the expression

$$v_0 \approx \frac{A\Omega_b C}{\sqrt{GB_{\text{ref}}}} = 0.15 \left(\frac{A}{3}\right) \left(\frac{\Omega_b}{2 \times 10^{-14} \text{ rad s}^{-1}}\right) \times \left(\frac{C}{0.19 \text{ km s}^{-1}}\right) \left(\frac{B_{\text{ref}}}{30 \mu\text{G}}\right)^{-1} \quad (2)$$

(see Basu 1997), where  $\Omega_b$  and  $B_{\text{ref}}$  are, respectively, the uniform background angular velocity and magnetic field strength. Based on the range of measured core angular velocities (see § 1),  $v_0$  could be a factor  $\sim 5$  larger or smaller than the fiducial value adopted in equation (2).

We assume that magnetic braking, which regulates the core rotation prior to its collapse, remains the dominant angular momentum transport mechanism also during the subsequent evolution. [A centrifugally driven disk wind may, however, dominate the angular momentum transport in the rotationally supported disk. In § 3 we argue that this is, indeed, a likely possibility, and in Appendix C we show that this mechanism can be incorporated into our model without significantly modifying the basic formulation.] We adopt the approach articulated by Basu & Mouschovias (1994) for the pre-PMF collapse phase. The torque per unit mass on the slab-like core (of surface mass density  $\Sigma$ ) can be approximated by  $rB_z B_{\phi,s}/2\pi\Sigma$ , where  $B_z$  is the vertical field component at the midplane and  $B_{\phi,s}$  is the azimuthal field component at the surface  $z = H$  (assuming  $H \ll r$ ). The latter can be estimated from the relation

$$B_{\phi,s}(r) = -\frac{\Psi(r)}{\pi r^2} \left( \frac{V_{i,\phi}(r) - r\Omega_b}{V_{\text{A,ext}}} \right), \quad (3)$$

where  $\Psi(r)$  is the magnetic flux threading the core within a radius  $r$ ,  $V_{i,\phi} = r\Omega_i$  is the azimuthal speed of the core ions, and  $V_{\text{A,ext}}$  is the speed with which the torsional Alfvén waves that effect the magnetic braking propagate in the external medium. Equation (3) is the same as equation (26) in Basu & Mouschovias (1994), where  $V_{\text{A,ext}}$  is also treated as a constant, except that we substituted the ion speed for the bulk (neutral) speed to take account of the possibility that the ions (into which the magnetic field is frozen) are not well coupled to the neutral core component (see Mouschovias & Paleologou 1986 and Königl 1987).

The assumption of a constant  $V_{\text{A,ext}}$  is consistent with theoretical models of magnetically supported clouds as well as with empirical data, which indicate that  $V_{\text{A,ext}} \approx 1 \text{ km s}^{-1}$  in molecular clouds over at least 4 orders of magnitude in density ( $\sim 10^3$ – $10^7 \text{ cm}^{-3}$ ; e.g., Crutcher 1999). This assumption

<sup>3</sup> As we discuss in § 3.2.3, we also do not expect the radial surface field component to greatly exceed the vertical field  $B_z$  under realistic circumstances.

is required for the construction of a self-similar model. In order for the steady-state expression (3) to be applicable, the Alfvén travel time in the external medium over the initial radius of the cloud should be less than the evolutionary time scale  $\sim r/|V_r|$  (which, for a rotationally supported disk, is essentially the local magnetic braking time). Our representative rotationally supported disk models typically have  $|V_r| \lesssim 0.1C$  (with  $|V_r| \rightarrow 0$  as  $r \rightarrow 0$ ), whereas, for a nominal temperature of 10 K,  $V_{\text{A,ext}}/C \approx 5$ . These estimates indicate that the assumption of rapid braking should not lead to gross errors even if it is not everywhere strictly correct. In our models we use the parameterization  $V_{\text{A,ext}} = C/\alpha$ , with  $\alpha = 0.1$  adopted as a typical value.

We will be interested in evaluating the effects of magnetic braking in regions where rotation already plays a dynamically significant role, so that  $\Omega_i \gg \Omega_b$ . We can therefore drop  $\Omega_b$  in equation (3), which will make it possible to incorporate this equation into a self-similar formulation. The anticipated increase in  $\Omega_i$  with decreasing  $r$  ( $\propto r^{-3/2}$  when a Keplerian disk is formed) will in general make  $B_{\phi,s}$  the dominant field component at the surface as the central point mass is approached. (This situation is not encountered in the pre-PMF phase; see Basu & Mouschovias 1994.) We expect, however, that various magnetohydrodynamic instabilities (in particular, internal kinks) will intervene to prevent the azimuthal field component from greatly exceeding the poloidal components.<sup>3</sup> We therefore impose a cap on the azimuthal field in the form  $|B_{\phi,s}| \leq \delta B_z$ . In our models we usually set  $\delta = 1$  — this choice, in fact, also corresponds to the typical value of  $|B_{\phi,s}|/B_z$  obtained in our model for a rotationally supported, diffusive disk when (as expected) the vertical angular momentum transport is dominated by a centrifugally driven wind (see § 4 and Appendix C).

## 2.2. Basic Equations

We represent the collapsing core as a thin disk surrounding a point mass  $M_c$ . We use cylindrical coordinates  $(r, \phi, z)$  centered on the point mass, with the disk midplane given by  $z = 0$ . The disk has a column density  $\Sigma$ , mass density  $\rho$ , and half-thickness  $H$  defined by  $\Sigma = 2H\rho$ . The total mass  $M(r)$  enclosed within the radius  $r$  is then given by  $M(r) = M_c + 2\pi \int_0^r \Sigma(r') r' dr'$ , and we denote its time derivative by  $\dot{M}$ . The disk velocity field  $\mathbf{V}(r)$  has radial and azimuthal components, with the latter giving rise to a specific angular momentum  $J = rV_\phi$ . We assume that the disk is threaded by an open magnetic field that is symmetric with respect to the midplane [i.e.,  $B_r = 0$  at  $z = 0$  and  $B_{r,s}(H) = -B_{r,s}(-H)$  at the disk surfaces ( $z = \pm H$ ), and similarly for  $B_\phi$ ]. The magnetic flux enclosed within the radius  $r$  is given by  $\Psi(r) = \Psi_c + 2\pi \int_0^r B_z(r') r' dr'$ , where  $\Psi_c$  denotes the flux trapped inside the central point mass.

In Appendix A we write down the basic disk equations, integrate them over  $z$  while retaining all terms of order  $H/r$ , and then go on to justify the omission of some of the  $\mathcal{O}(H/r)$  terms in the interest of greater simplification. The result of these manipulations is the following set of equations,

$$\frac{\partial \Sigma}{\partial t} + \frac{1}{r} \frac{\partial}{\partial r} (rV_r \Sigma) = 0, \quad (4)$$

$$\frac{\partial V_r}{\partial t} + V_r \frac{\partial V_r}{\partial r} = g_r - \frac{C^2}{\Sigma} \frac{\partial \Sigma}{\partial r} + \frac{B_z}{2\pi \Sigma} \left( B_{r,s} - H \frac{\partial B_z}{\partial r} \right) + \frac{J^2}{r^3}, \quad (5)$$

$$\frac{\partial J}{\partial t} + V_r \frac{\partial J}{\partial r} = \frac{rB_z B_{\phi,s}}{2\pi \Sigma}, \quad (6)$$

and

$$\frac{\Sigma C^2}{2H} = \frac{\pi}{2} G \Sigma^2 + \frac{G M_c \rho H^2}{2r^3} + \frac{1}{8\pi} \left( B_{\phi,s}^2 + B_{r,s}^2 - B_{r,s} H \frac{\partial B_z}{\partial r} \right), \quad (7)$$

which express mass, radial momentum, and angular momentum conservation, and vertical hydrostatic equilibrium, respectively.

Under the assumption that the magnetic field evolution is governed by ambipolar diffusion, one can regard the magnetic field lines as being frozen into the ions. The latter move with velocity  $\mathbf{V}_i$  and drift with respect to the bulk (neutral) gas component at the drift velocity  $\mathbf{V}_D \equiv \mathbf{V}_i - \mathbf{V}$ . By balancing the Lorentz force on the ions with the ion-neutral collisional drag force, one can solve for the components of  $\mathbf{V}_D$ :

$$V_{D,r} = \frac{\tau_{ni} B_z}{2\pi \Sigma} \left( B_{r,s} - H \frac{\partial B_z}{\partial r} \right), \quad (8)$$

$$V_{D,\phi} = \frac{\tau_{ni} B_z B_{\phi,s}}{2\pi \Sigma}. \quad (9)$$

We then have

$$\frac{\partial \Psi}{\partial t} = -2\pi r V_{i,r} B_z = -2\pi r (V_r + V_{D,r}) B_z. \quad (10)$$

As in CCK, we adopt the monopole approximations for  $g_r$  and  $B_{r,s}$ ,

$$g_r = -\frac{GM(r,t)}{r^2}, \quad (11)$$

$$B_{r,s} = \frac{\Psi(r,t)}{2\pi r^2}, \quad (12)$$

which considerably simplify the calculations and are not expected to introduce any significant errors (see also Li & Shu 1997, Saigo & Hanawa 1998, CK, and Tsuribe 1999).

For the azimuthal magnetic field component, we use equation (3) in the limit  $V_{i,\phi}/r \gg \Omega_b$  together with equation (9), and impose the bounding condition on  $|B_{\phi,s}|$  discussed at the end of § 2.1. We then obtain

$$B_{\phi,s} = -\min \left[ \frac{\Psi}{\pi r^2} \frac{V_\phi}{V_{A,\text{ext}}} \left( 1 + \frac{\Psi B_z \tau_{ni}}{2\pi^2 r^2 \Sigma V_{A,\text{ext}}} \right)^{-1}; \delta B_z \right]. \quad (13)$$

### 2.3. Self-Similar Equations in Nondimensional Form

We introduce a similarity variable  $x$  and a set of nondimensional flow quantities that depend only on  $x$ :

$$x = r/Ct, \quad (14)$$

$$H(r,t) = Ct h(x), \quad \Sigma(r,t) = (C/2\pi Gt) \sigma(x), \quad (15)$$

$$V_r(r,t) = Cu(x), \quad V_\phi(r,t) = Cv(x), \quad (16)$$

$$g_r(r,t) = (C/t) g(x), \quad J(r,t) = C^2 t j(x), \quad (17)$$

$$M(r,t) = (C^3 t/G) m(x), \quad \dot{M}(r,t) = (C^3/G) \dot{m}(x), \quad (18)$$

$$\mathbf{B}(r,t) = (C/G^{1/2} t) \mathbf{b}(x), \quad \Psi(r,t) = (2\pi C^3 t/G^{1/2}) \psi(x). \quad (19)$$

These definitions extend the set used in CCK to the rotational case (which involves the dimensionless azimuthal speed  $v$  and specific angular momentum  $j$ ) — note, however, that the variables  $h$ ,  $u$ ,  $\sigma$ , and  $\mu \equiv \sigma/b_z$  in the present paper were denoted by  $\hat{h}$ ,  $v$ ,  $a$ , and  $\lambda$ , respectively, in CCK. To help relate our results to real protostellar systems, we observe that, for our fiducial value of  $C (= 0.19 \text{ km s}^{-1})$ ,  $x = 1$  corresponds to a distance

$r \approx 6 \times 10^{15} \text{ cm} (= 400 \text{ AU})$  when  $t = 10^4 \text{ yr}$  (the characteristic age of a Class 0 YSO) and to a distance  $r \approx 6 \times 10^{16} \text{ cm} (= 4000 \text{ AU})$  when  $t = 10^5 \text{ yr}$  (the characteristic age of a Class I YSO).

CCK demonstrated that ambipolar diffusion can be incorporated into a self-similar model when  $\rho_i \propto \rho^{1/2}$ . When rotation is present, we find that magnetic braking can similarly be included if  $V_{A,\text{ext}} = \text{const}$ . The nondimensional model parameters that control the strength of these two effects are  $\eta$  and  $\alpha$ , respectively (see § 2.1). [A self-similar formulation is also possible if angular momentum transport is due to an “ $\alpha$  viscosity,”  $\nu = \alpha_{\text{SS}} CH$  (Shakura & Sunyaev 1973), when  $C$  and the parameter  $\alpha_{\text{SS}} (\lesssim 1)$  are constant. This was noted by Tsuribe (1999) in the special case where  $H$  has the value appropriate to a Keplerian disk, and by Mineshige & Umemura (1997) in the case when  $H$  has the value appropriate to a self-gravitating disk (although the latter authors required  $\alpha_{\text{SS}} H/r$ , rather than  $\alpha_{\text{SS}}$ , to be a constant).] With the above expressions for the similarity variables, and defining also  $w \equiv x - u$  for convenience, the structure equations can be rewritten in the following nondimensional, self-similar form:

$$\frac{dw}{dx} = w \left( \frac{1}{\sigma} \frac{d\sigma}{dx} + \frac{1}{x} \right), \quad (20)$$

$$(1 - w^2) \frac{1}{\sigma} \frac{d\sigma}{dx} = g + \frac{b_z}{\sigma} \left( b_{r,s} - h \frac{db_z}{dx} \right) + \frac{j^2}{x^3} + \frac{w^2}{x}, \quad (21)$$

$$\psi - xwb_z + \eta x b_z^2 h^{1/2} \sigma^{-3/2} \left( b_{r,s} - h \frac{db_z}{dx} \right) = 0, \quad (22)$$

$$\frac{dj}{dx} = w^{-1} (j - x b_z b_{\phi,s} / \sigma), \quad (23)$$

$$b_{\phi,s} = -\min \left\{ \frac{2\alpha \psi j}{x^3} \left( 1 + \frac{2\alpha \eta h^{1/2} \psi b_z}{\sigma^3 / 2x^2} \right)^{-1}; \delta b_z \right\}, \quad (24)$$

$$m = xw\sigma, \quad (25)$$

$$\dot{m} = -xu\sigma, \quad (26)$$

$$\frac{dm}{dx} = x\sigma, \quad (27)$$

$$\frac{d\psi}{dx} = x b_z, \quad (28)$$

$$g = -m/x^2, \quad (29)$$

and

$$b_{r,s} = \psi/x^2. \quad (30)$$

The disk half-thickness  $h$  can be found from the vertical hydrostatic equilibrium condition, which yields

$$\left( \frac{\sigma m_c}{x^3} - b_{r,s} \frac{db_z}{dx} \right) h^2 + (b_{r,s}^2 + b_{\phi,s}^2 + \sigma^2) h - 2\sigma = 0. \quad (31)$$

The solution of this quadratic equation is

$$h = \frac{\hat{\sigma} x^3}{2\hat{m}_c} \left[ -1 + \left( 1 + \frac{8\hat{m}_c}{x^3 \hat{\sigma}^2} \right)^{1/2} \right], \quad (32)$$

where  $\hat{m}_c \equiv m_c - x^3 b_{r,s} (db_z/dx)/\sigma$  and  $\hat{\sigma} \equiv \sigma + (b_{r,s}^2 + b_{\phi,s}^2)/\sigma$ . Equation (32) implies that  $h \rightarrow 2/\sigma$ ,  $(2/m_c)^{1/2} x^{3/2}$ , and  $2\sigma/[b_{r,s}^2 + b_{\phi,s}^2]$  in the limits where self-gravity, central-mass

gravity, and magnetic stresses, respectively, dominate the vertical squeezing of the disk.<sup>4</sup>

As discussed in § 2.1, the initial ( $t = 0$ ) conditions [which in the self-similar model also represent the outer asymptotic ( $r \rightarrow \infty$ ) values] correspond to a collapsing core just before PMF. Thus we require

$$\sigma \rightarrow \frac{A}{x}, \quad b_z \rightarrow \frac{\sigma}{\mu_0}, \quad u \rightarrow u_0, \quad v \rightarrow v_0 \quad \text{as } x \rightarrow \infty, \quad (33)$$

where  $A$ ,  $\mu_0$ ,  $u_0$ , and  $v_0$  are constants. As discussed in § 2.1, our fiducial values for  $A$  ( $= 3$ ) and  $u_0$  ( $= -1$ ) are the same as those used by CCK; they are based on the results of numerical simulations of nonrotating cores and are compatible with observations. We similarly adopt the CCK choice  $\mu_0 = 2.9$ . Our reference values for the uniform initial rotation  $v_0$  are based on the range of measured core angular velocities and typical cloud parameters that enter into the estimate (2).

### 3. RESULTS

We have studied three distinct cases of rotational core collapse, which we present in this section in order of increasing complexity. They are: (1) A purely hydrodynamical collapse, with no mechanism for angular momentum transport (§ 3.1); (2) An ideal-MHD (IMHD) collapse, which incorporates magnetic braking but does not include any magnetic field diffusivity that could prevent the buildup of a central magnetic monopole (§ 3.2); (3) an MHD collapse that includes ambipolar diffusion (AD; § 3.3). The latter model is able to reproduce the basic observational features of rotationally supported protostellar disks and their central YSOs.

Our models have many features in common, arising from the basic interplay between the centrifugal force and gravity. Initially and at large distances from the center (i.e., for large values of  $x$ ), gravity is stronger than the centrifugal force and matter falls in at a high, supersonic speed. In this regime  $m \gg m_c$ , and self-gravity dominates over attraction by the central object. A very different behavior characterizes small values of  $x$ . Typically, the innermost region constitutes a Keplerian accretion disk, where gravity approximately balances the centrifugal force and where the infall speed is low and subsonic. The transition between the supersonic and subsonic inflow regimes is achieved through a shock, which is located at the point ( $x_c$ ) where the infalling matter encounters a centrifugal barrier. Inward of this shock the column density increases significantly, forming a dense accretion disk. The location of the centrifugal shock roughly coincides with the *centrifugal radius*, which is the largest radius where the gravitational ( $-m/x^2$ ) and centrifugal ( $j^2/x^3$ ) accelerations are in approximate balance (e.g., Basu 1998). In fact, we find that the point where the equality  $j^2(x)/m(x) = x$  is first satisfied as the matter flows in yields a value that is only a slight ( $\sim 4\%$ ) overestimate of the actual shock location in both the IMHD and AD cases when (as is the case in our typical models)  $m(x_c) \approx m_c$ . The value of the centrifugal radius is sometimes estimated from the  $t = 0$  expressions for the surface density and angular momentum profiles. This estimate could be rather inaccurate since it does not account for the mass accumulation at the center or for the loss of angular momentum that the infalling matter experiences even before it reaches the centrifugal radius. We discuss more accurate estimates of  $x_c$  in the following subsections.

<sup>4</sup> CCK employed an expression similar to equation (31), except that they omitted the magnetic terms. Their solution for  $h$  thus has the same form as equation (32), but with  $\dot{m}_c$  and  $\dot{\sigma}$  replaced by  $m_c$  and  $\sigma$ , respectively.

Our “standard” solutions, corresponding to the fiducial parameter values, are presented in § 3.2.1 for the IMHD case and in § 3.3.1 for the AD case. We also present solutions in the limit when the initial rotation is very fast and magnetic braking is either nonexistent (§ 3.1) or comparatively inefficient (§ 3.2.2 and § 3.3.2 for the IMHD and AD cases, respectively). Under these conditions the rotationally supported disk becomes fairly extended and its mass greatly exceeds that of the central object. Another “extreme” type of a solution is obtained in the opposite limit, when the initial rotation is braked so efficiently that  $j$  is effectively reduced to zero at a finite value ( $x_j$ ) of  $x$ . In this limit, too, we present solutions for both the IMHD (§ 3.2.3) and AD (§ 3.3.3) cases. These configurations are effectively nonrotating (and thus resemble the CCK solutions) for  $x < x_j$ , and they do not feature either a centrifugal radius or a Keplerian accretion disk; instead, matter accretes directly onto the central object at a supersonic speed.

#### 3.1. Nonmagnetic Rotational Collapse

This problem was already treated in detail by Saigo & Hanawa (1998); it is included here for reference and comparison, and to serve as a starting point.

In the absence of magnetic fields or of any other means of angular momentum transport, the self-similar collapse is characterized by  $j/m = \Phi$ , where  $\Phi$  is a constant fixed by the initial conditions ( $\Phi = v_0/A$ ). The inner asymptotic solution ( $x \rightarrow 0$ ) is given by  $\sigma = E/x$  and  $m = Ex$ , with  $E \equiv [1 + (1 - 4\Phi^2)^{1/2}]/(2\Phi^2)$ . Numerically, we proceed by applying the initial conditions at  $x_{\max} = 10^2$  and integrating the differential equations toward smaller values of  $x$  until the expected location of  $x_c$  (see eq. [36] below) is reached. There we impose the isothermal shock jump condition described in Appendix B.1, and continue the integration until the asymptotic solution is approximately fulfilled. The exact value of  $x_c$  is obtained iteratively by enforcing the matching to this asymptotic solution to a high precision.

Figures 1 and 2 show profiles of mass, column density, and radial speed for two kinds of initial rotation: a typical ( $v_0 = 0.1$ ) and a rapid ( $v_0 = 1$ ) one. In both cases the centrifugal shock is very abrupt, producing a large increase in column density and a sudden decrease in inflow speed. In the case with faster initial rotation, the effect of the centrifugal barrier is so strong that it forces the radial velocity  $u$  to change sign below  $x_c$  to  $u > 0$  (indicating a backflow), as shown in Figure 2. The centrifugal shock thus separates regions of infall and backflow; it stays stationary in self-similar coordinates, implying that it moves outward in physical space. This phenomenon was already discussed in Saigo & Hanawa (1998). By trying a few other values of  $v_0$  (but keeping the other parameter values unchanged), we have found that  $v_0 = 0.5$  is too small to produce a backflow but that  $v_0 = 0.8$  is already large enough.

An interesting behavior exhibited by these solutions (and standing out particularly in Fig. 1) is the development of a mass “plateau” when the infall speed starts to increase above its outer asymptotic ( $x \gg 1$ ) value. This behavior is generic to all except our fast-rotation solutions (§ 3.2.2 and § 3.3.2) and can be understood as follows. According to equations (25) and (26),  $m = \sigma x(x - u)$  and  $\dot{m} = -\sigma x u$ . These equations are consistent with the outer asymptotic solution  $m = Ax = \sigma x^2$  and  $u = u_0 < 0$  (eq. [33]) only so long as  $x \gg |u|$  (in which case  $m \gg \dot{m}$ ). This

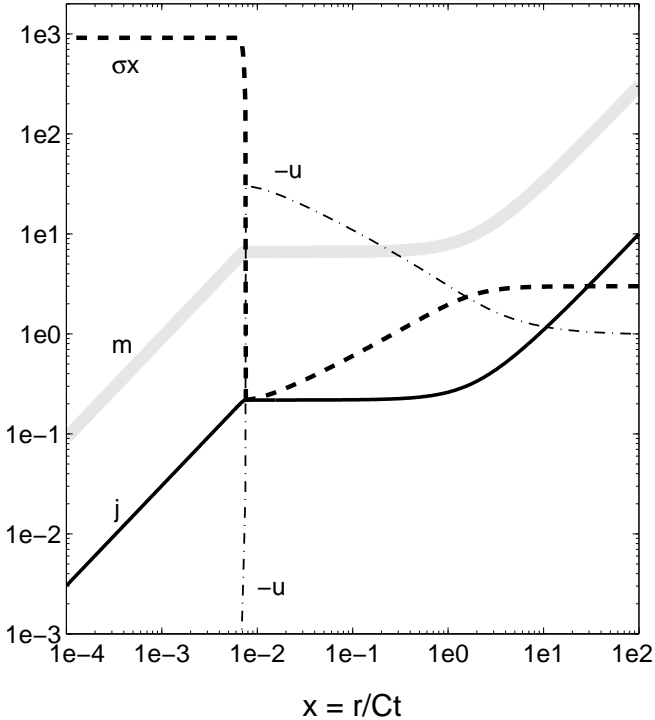


FIG. 1.— Self-similar solution for a nonmagnetic rotational collapse. The variations of the normalized radial infall speed  $-u$ , surface density  $\sigma$ , and total mass  $m$  are plotted as functions of the similarity variable  $x$ . The initial (or outer asymptotic boundary) conditions correspond to the parameter values  $v_0 = 0.1$ ,  $A = 3$ , and  $u_0 = -1$ . The centrifugal shock is located at  $x_c = 7.5 \times 10^{-3}$ . No central mass forms in this case on account of the assumed lack of any angular-momentum transport mechanism.

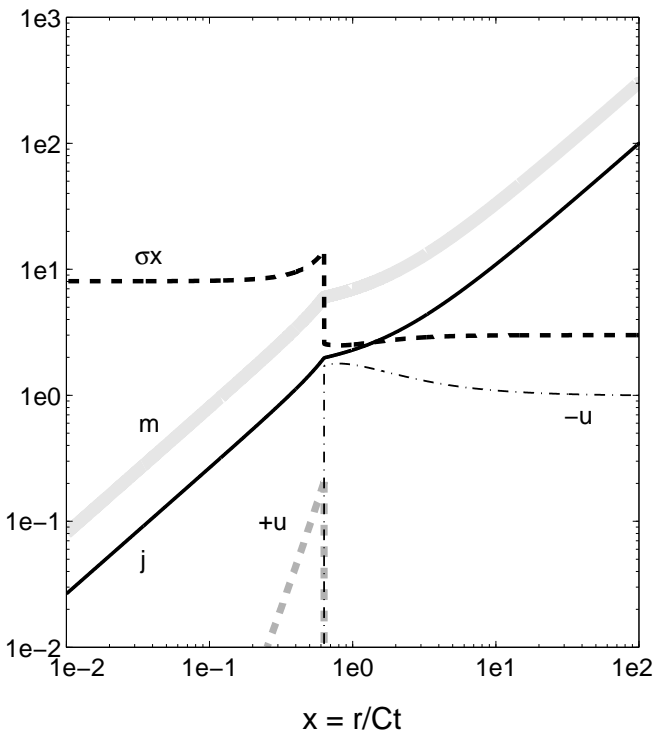


FIG. 2.— Same as Fig. 1, except that the azimuthal-velocity parameter  $v_0$  is increased from 0.1 to 1. Note the change in the sign of  $u$  across the centrifugal shock in this case and the comparatively large value of  $x_c (=0.63)$ .

inequality breaks down when  $x$  becomes small enough that it drops below  $|u|$ . This point marks the approximate outer edge of the mass plateau, and we label it  $x_{\text{pl}}$ . Its value can be estimated by setting

$$x_{\text{pl}} \approx |u_0|, \quad (34)$$

although typically  $|u|$  is already somewhat larger than  $|u_0|$  at that point. The plateau mass can then be approximated by

$$m_{\text{pl}} \approx (A/x_{\text{pl}})x_{\text{pl}}(x_{\text{pl}} - u_0) \approx 2|u_0|A. \quad (35)$$

For  $x \ll x_{\text{pl}}$ ,  $|u| \gg x$ , and hence  $m \approx \dot{m}$  and (using eq. [27])  $dm/dx = \sigma x \ll m/x$ . The latter inequality accounts for the appearance of the plateau in the logarithmic plots of  $m$  vs.  $x$ . If  $x_c/x_{\text{pl}}$  is sufficiently small, then, in the plateau regime,  $|u|$  approaches the free-fall value corresponding to  $m \approx m_{\text{pl}}$ . Hence, once  $|u|$  comes to exceed  $x$ , their ratio increases rapidly with decreasing  $x$ , and the mass plateau is quickly established. The derivation of equations (34) and (35) is independent of the degree of magnetization of the flow, and the expression (35) therefore also provides an excellent first guess of  $m_c$  in our fiducial magnetic solutions that involve point-mass formation. These results do not, however, apply to the fast-rotation cases considered in § 3.2.2 and § 3.3.2, where a plateau does not form because the centrifugal shock is established before  $x$  becomes  $\ll |u|$ , and where the central mass is typically smaller than that of the disk.

Setting  $j/m = \Phi$  and  $m \approx m_{\text{pl}}$  in the expression  $x_c \approx (j/m)^2 m$ , we infer

$$x_c \approx 2|u_0|v_0^2/A. \quad (36)$$

We have used this expression to obtain the initial guess in our numerical calculation. For the parameters of Figure 1, this gives  $x_c \approx 7 \times 10^{-3}$ , which is seen to be an excellent approximation to the actual value. This estimate is only applicable if  $x_c \lesssim x_{\text{pl}}$ , i.e., for  $v_0 \lesssim (A/2)^{1/2}$ . This condition is still marginally satisfied in the solution presented in Figure 2.

The inner asymptotic solution of this model precludes the formation of a point mass. As the azimuthal speed  $v$  cannot diverge as  $x \rightarrow 0$ ,  $j = vx$  must vanish at the origin. To form a central object with  $m_c \neq 0$ , a braking mechanism that allows  $j/m$  to decrease as  $x \rightarrow 0$  is required. The absence of such a mechanism explains the linear decline of  $m$  with  $x$  at small values of  $x$  (which for the parameters used in Figs. 1 and 2 effectively starts already at  $x_c$ ). It may also be expected that a braking mechanism will lead to a more gradual radial deceleration, reducing or even altogether preventing the backflow exhibited by the rapid-rotation solution shown in Figure 2. In the following subsections we examine to what extent these expectations are met in the presence of magnetic braking.

### 3.2. Ideal-MHD Rotational Collapse

In this section we present an IMHD model for magnetic braking based on the formalism described by equations (20)–(31), in which we set  $\eta = 0$ .

The existence of a braking mechanism leads to a qualitative change in the character of the solutions. In contrast to the nonmagnetic solution presented in § 3.1,  $j/m$  is not a constant in this case, and magnetic braking allows a central mass to form despite the initial presence of rotation.

Flux freezing under the ideal-MHD assumption implies that  $b_z = \sigma/\mu$  and  $\psi = m/\mu$ , where  $\mu$ , the nondimensional mass-to-flux ratio, is a constant (equal to its initial value  $\mu_0$ ). It is also convenient to introduce the auxiliary constant  $\bar{\mu} \equiv (1 - \mu^{-2})^{1/4}$ ,

which is useful for describing the effect of the magnetic “dilution” of the gravitational field (Shu & Li 1997).

There are two qualitatively different sets of asymptotic relations for the inner region ( $x \rightarrow 0$ ) of this model. The first set, presented in equations (37)–(42) below, applies to the configurations described in § 3.2.1 and § 3.2.2. The second set, presented in § 3.2.3, applies only in the strong-braking case. Both of these sets describe the formation of a dynamically dominant central mass and a split-monopole field. However, the first set represents a rotationally supported disk, whereas the second one depicts a nonrotating, supersonic inflow.

The disk-like inner asymptotic solution is

$$\dot{m} = m = m_c, \quad (37)$$

$$j = \bar{\mu}^2 m_c^{1/2} x^{1/2}, \quad (38)$$

$$-u = w = (2\delta)^{1/2} m_c^{1/4} \mu^{-1} \bar{\mu}^{-1} x^{1/4}, \quad (39)$$

$$-b_{\phi,s}/\delta = b_z = \sigma/\mu = \bar{\mu} m_c^{3/4} (2\delta)^{-1/2} x^{-5/4}, \quad (40)$$

$$b_{r,s} = \psi/x^2 = m_c/(\mu x^2), \quad (41)$$

$$h = 2\sigma/b_{r,s}^2 = \bar{\mu} \mu^3 m_c^{-5/4} (2/\delta)^{1/2} x^{11/4}. \quad (42)$$

These equations represent an essentially Keplerian disk; in particular, the expression for  $j$  differs from that of a purely Keplerian system only by the magnetic-dilution factor  $\bar{\mu}^2$  [which, however, remains close to 1 ( $\approx 0.94$ ) for our fiducial value of  $\mu_0$ ]. The  $j$  profile corresponding to such a disk implies that  $j/m$  decreases with decreasing  $x$ . The magnetic braking required to account for this change from the initial distribution fixes the strength and radial power-law index of the magnetic field components  $b_z$  and  $b_{\phi,s}$ . The flux-freezing condition then determines the value of  $\sigma$ , and the mass conservation relation, in turn, yields the expression for  $u$ .

The behavior of the IMHD solutions is determined primarily by the magnitude of the initial rotation and the strength of the magnetic braking. We consider three qualitatively different cases: a typical collapse in which both effects are relevant over most scales (§ 3.2.1); a limiting case corresponding to weak braking and fast rotation (§ 3.2.2); and another limiting case in which very strong braking is capable of eliminating rotation altogether by the time the flow reaches a finite distance from the origin, resulting in the formation of an inner nonrotating-inflow zone (§ 3.2.3).

The method used to solve the differential equations is essentially the same as that used in § 3.1. For the initial guess of the value of  $x_c$  we again use the estimate (36). Although magnetic braking does operate in this case, the deviation of  $j/m$  from its  $x \gg 1$  asymptotic value remains relatively small in the range  $x > x_c$ , and the approximation obtained for the nonmagnetic case remains fairly good (as evidenced by the fact that the value of  $x_c$  in the solution presented in Fig. 3 differs by a factor of less than 2 from its value in Fig. 1). The discontinuities in the variables  $\sigma$ ,  $b_z$ , and  $u$  across the shock are estimated using the appropriate shock jump conditions. For the typical case (§ 3.2.1) the shock occurs in a region where  $h \approx 2\sigma/b_{r,s}^2$ , and the “magnetically squeezed shock” jump conditions described in Appendix B.3 are applicable. In the fast-rotation case (§ 3.2.2) the shock is located sufficiently far away from the origin that a generalized (to include magnetic effects) isothermal shock (Appendix B.2) provides a better approximation. (The issue of shock jump conditions is not relevant to the strong-braking inflow considered in § 3.2.3, since no centrifugal shock forms in that case.) As in § 3.1, a successful convergence of the solution at  $x < x_c$  to its asymptotic ( $x \rightarrow 0$ ) form requires a correct se-

lection of the point  $x_c$ , which is achieved iteratively. (Incorrect choices of  $x_c$  produce numerical solutions with a spontaneous singularity at some point  $0 < x < x_c$ , similar to those found in Li 1998.) As the value of the central mass is not known before the numerical integrations start, we adopt  $m_c \approx m_{\text{pl}}$  (eq. [35]) as an initial guess that is refined iteratively until convergence is attained.

### 3.2.1. Fiducial Solution

The results for this case are presented in Figure 3. For the fiducial parameters  $v_0 = 0.1$ ,  $\alpha = 0.1$ , and  $\delta = 1$ , rotation and braking are both moderate. Magnetic braking is strong enough to prevent shock formation in the region where self-gravity dominates (as in § 3.2.2), but it is not so strong as to prevent the shock from forming altogether (as in § 3.2.3). The centrifugal shock thus occurs well inside the region where the central mass dominates the gravitational field, with  $m(x_c) \approx m_c$ . The disk that forms for  $x < x_c$  is thus essentially Keplerian and has an angular momentum profile  $j \propto x^{1/2}$ . The large inclination of the magnetic field lines to the disk surface indicated by the inner asymptotic solution ( $b_{r,s}/b_z \propto x^{-3/4}$  as  $x \rightarrow 0$ ; see eqs. [40] and [41]) suggests that the disk would likely drive a centrifugal wind from its surfaces, which would reduce  $m_c$ . We neglect this effect in the present discussion, but we consider it in § 4 and Appendix C in relation to the ambipolar-diffusion fiducial solution.

The evolution of the inflow can be characterized by dividing the range of  $x$  into four regions, which are, in order of decreasing distance from the center:

**Self-gravity-dominated region.** For the largest values of  $x$ , the initial value of the ratio  $j/m$  ( $= 0.033$ ) is still conserved, and  $m$ , which is still much larger than its central value, is proportional to  $x$ .

**Free-fall region.** After a transition region, where  $j/m$  decreases slightly from its initial value on account of magnetic braking, both  $m$  and  $j$  enter a plateau (at  $x \approx x_{\text{pl}}$ ; see eq. [34]). They become independent of  $x$ , with values  $m_{\text{pl}} = 6.2$  and  $j_{\text{pl}} = 0.18$  (corresponding to  $j/m = 0.028$ ). These computed values can be substituted into the expression  $x_c \approx j_{\text{pl}}^2/m_{\text{pl}}$  to provide a refinement of the estimate (36) for the location of the centrifugal shock. As can be seen from a comparison of this value with the computed result (listed in the caption to Fig. 3), the approximation is excellent (as is the correspondence between the value of  $m_{\text{pl}}$  and that of  $m_c$ ). Near the inner edge of this region, the centrifugal force starts to exceed gravity.

**The centrifugal shock.** The outer edge of this region is where the variables  $\sigma$ ,  $u$ , and  $b_z$  undergo the discontinuities prescribed by the shock jump conditions of Appendix B.3. Just inside the discontinuity the column density becomes very large, but it then rapidly decreases toward its asymptotic near-Keplerian value. The infall speed decreases rapidly, but not so strongly as to produce any backflow (i.e.,  $u$  remains  $< 0$  for all  $x$ ). It is in this postshock transition zone that the angular momentum makes the final adjustment to its asymptotic, magnetically diluted, Keplerian value: this sudden bout of braking is triggered by the spike in  $b_z$  that results from the shock compression. The column density spike that occurs in this region is associated with a small (but finite) mass,  $\Delta m \approx 0.02$ , which



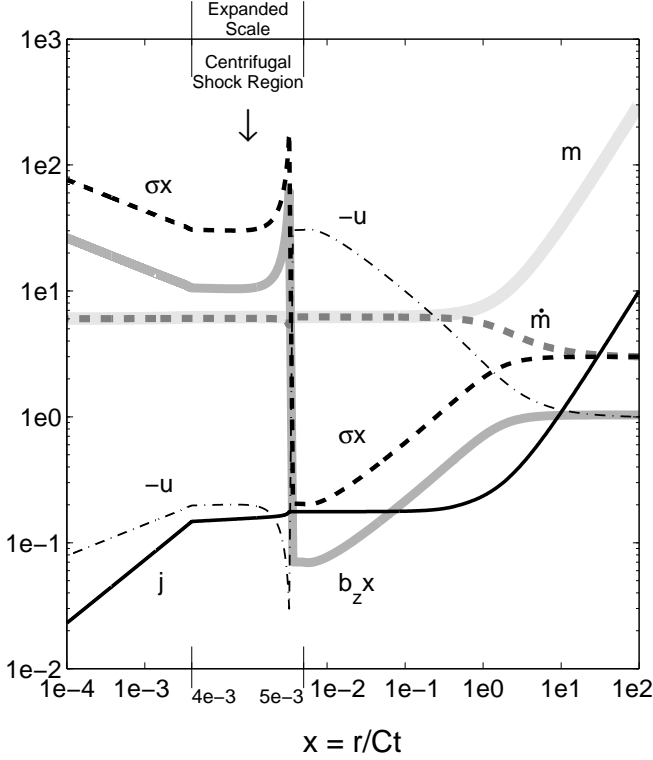


FIG. 3.— Fiducial solution for an ideal-MHD rotational collapse. The variations of the normalized radial infall speed  $-u$ , surface density  $\sigma$ , total mass  $m$ , mass accretion rate  $\dot{m}$ , specific angular momentum  $j$ , and  $z$  component of the magnetic field  $b_z$  are plotted as functions of the similarity variable  $x$ . The initial (or outer asymptotic boundary) conditions correspond to the parameter values  $v_0 = 0.1$ ,  $A = 3$ ,  $u_0 = -1$ , and  $\mu_0 = 2.9$ , whereas the magnetic-braking model parameters are  $\alpha = 0.1$  and  $\delta = 1$ . The centrifugal shock is located at  $x_c = 4.9 \times 10^{-3}$ , and the horizontal scale in its vicinity has been expanded to show details of the postshock transition zone. The central mass is  $m_c = 6.0$ .

could be pictured as a massive ring located at the edge of the Keplerian disk. After undergoing fast variations as it transits through this region, the flow merges seamlessly into the next, smoothly varying zone.

**Magnetically diluted Keplerian disk.** In this region, the asymptotic equations (37)–(42) are satisfied. The rotationally supported disk has a mass  $m_d \approx 3.2\%$  of  $m_c$  and is in an almost perfect dynamical equilibrium, as the inflow speed is low ( $\lesssim 0.2C$ ).

### 3.2.2. Fast Rotation

If the initial azimuthal speed  $v_0$  is high and the braking parameters  $\alpha$  and  $\delta$  are moderate or small, then the value of  $j$  can become quite high, which can lead to a large value of the centrifugal radius  $x_c$ . In an extreme case, the centrifugal shock may occur so far away from the center that it is located within the self-gravity-dominated region, where  $m \gg m_c$ .

Figures 4 and 5 show two solutions, corresponding to a fast initial rotation ( $v_0 = 1.5$ ) and two different values of the braking parameter  $\alpha$  (0.01 and 0.1, respectively;  $\delta = 1$  in both cases). The centrifugal shock in these solutions is so strong that the radial speed  $u$  changes sign across the shock. This is similar to the backflow observed for large values of  $j$  in the absence of braking (see Fig. 2) and is consistent with the expectation that the braking must be strong enough to qualitatively change the behavior of a rapidly rotating inflow. The backflow region in

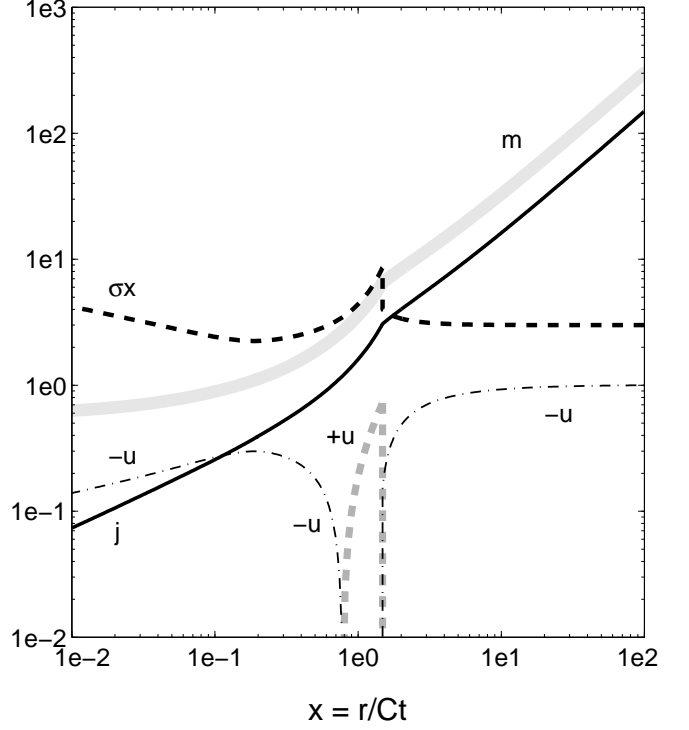


FIG. 4.— Fast-rotation solution for an ideal-MHD rotational collapse. The variations of the normalized radial infall speed  $-u$ , surface density  $\sigma$ , total mass  $m$ , and specific angular momentum  $j$  are plotted as functions of the similarity variable  $x$ . The model parameter values are the same as in the fiducial case (Fig. 3), except that the azimuthal-velocity parameter  $v_0$  is increased from 0.1 to 1.5. In this case the centrifugal-shock radius is comparatively large ( $x_c = 1.48$ ) and the central mass is rather small ( $m_c = 0.57$ ). A backflow layer ( $u > 0$ ) is present just inside the centrifugal shock: within this layer, the velocity curve depicts  $+u$  instead of  $-u$ .

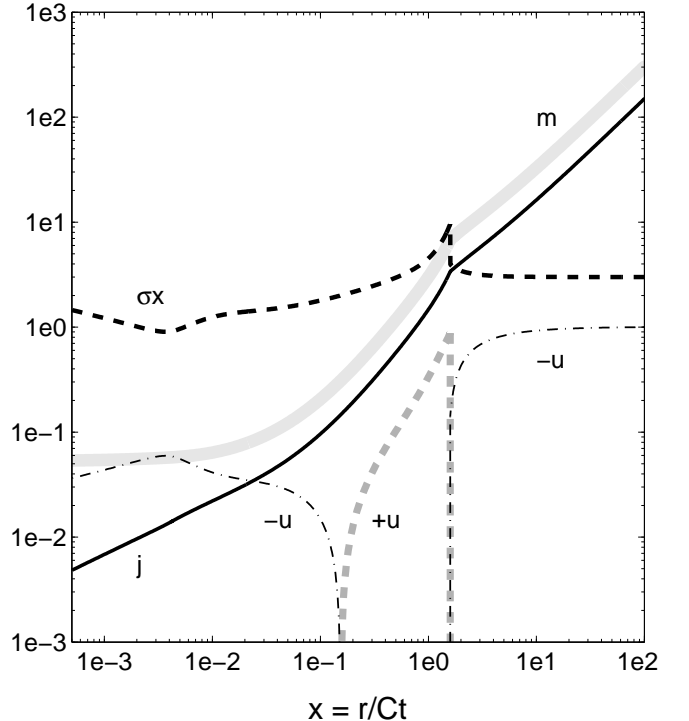


FIG. 5.— Same as Fig. 4, except that the braking parameter  $\alpha$  is decreased from 0.1 to 0.01. This results in a wider backflow layer and a smaller Keplerian-rotation region. The centrifugal shock location is not much changed ( $x_c = 1.53$ ), but the central mass is strongly reduced ( $m_c = 0.05$ ).

this case is clearly seen to occupy only a finite range in  $x$  and not to reach all the way to the origin: it represents an annulus, interior to which the infall resumes.

The large values of  $x_c$  result in extended, and hence fairly massive, disks. On the other hand, the comparatively weak braking inhibits mass accumulation at the center: the central masses obtained in these solutions (listed in the captions to Figs. 4 and 5) are much smaller than the mass derived for the fiducial parameters in § 3.2.1 (which, in turn, is comparable to  $m_c$  in the nonrotating collapse model of CCK). The outer regions of the disks are therefore manifestly non-Keplerian. (The specific angular momentum approaches to within  $\sim 20\%$  of the asymptotic, diluted-Keplerian value given by eq. [38] only when  $x$  decreases below  $\sim 0.11x_c$  for the solution in Fig. 4 and below  $\sim 0.04x_c$  for the solution in Fig. 5.) As can be seen from a comparison of Figures 4 and 5, a larger value of the braking parameter  $\alpha$  leads to a reduction in  $j$  and results in the value of  $x_c$  becoming smaller and that of  $m_c$  larger. Correspondingly, the width of the backflow region is reduced and the Keplerian regime extends further out. These trends continue as the effect of rotation is diminished: by the time the parameters attain their fiducial values, the backflow region has completely disappeared and the inner asymptotic solution starts very close to  $x_c$ .

In summary, the collapse of fast-rotating cores that lack an exceptionally strong braking mechanism results in fairly massive disks and in comparatively low-mass central objects. The disks are rotationally supported and largely self-gravitating, with only their innermost regions exhibiting Keplerian behavior.

### 3.2.3. Strong Braking

If braking is very efficient then the innermost region of the inflow can have effectively zero angular momentum even if the collapsing core starts out rotating. This situation is illustrated in Figure 6, which depicts a solution with a fairly respectable initial rotation ( $v_0 = 1$ ) but with extreme values of the braking parameters ( $\alpha = \delta = 10$ ), which give rise to a strong surface azimuthal field (see eq. [24]). In this case the angular momentum is reduced effectively to zero at  $x_j \approx 0.2$ , before a centrifugal shock could occur, and thus no rotationally supported disk is formed. For  $x < x_j$ ,  $j = b_{\phi,s} = 0$ , and as  $x \rightarrow 0$ , the inflow tends to the asymptotic form of the nonrotating magnetic solution derived by CCK (see their §3.3). In this limit the flow becomes a supersonic, magnetically diluted free fall onto the central mass:

$$\dot{m} = m = m_c, \quad (43)$$

$$-u = [2m_c(1 - \mu^{-2})/x]^{1/2}, \quad (44)$$

$$\sigma = \mu b_z = [m_c/2(1 - \mu^{-2})x]^{1/2}, \quad (45)$$

$$b_{r,s} = \psi/x^2 = m_c/(\mu x^2), \quad (46)$$

$$h = 2\sigma/b_{r,s}^2 = \mu^2[2/m_c^3(1 - \mu^{-2})]^{1/2} x^{7/2}. \quad (47)$$

The numerical solution converges to these asymptotic values already quite close to  $x_j$  (at  $x \sim 0.1$ ).

Equation (47) for the disk scale height shows the strong effect of magnetic squeezing by the radial magnetic field component in the asymptotic solution. (Since the radial surface magnetic field scales as  $x^{-2}$ , it dominates the magnetic terms in both the vertical and the radial force-balance equations.) The dependence of  $h$  on  $x$  ( $\propto x^{7/2}$ ) is much stronger than in the solution presented by CCK ( $h \propto x^{3/2}$ ), in which the effect of magnetic pinching was neglected. However, apart from this difference, these two solutions are very similar; in particular, the value of

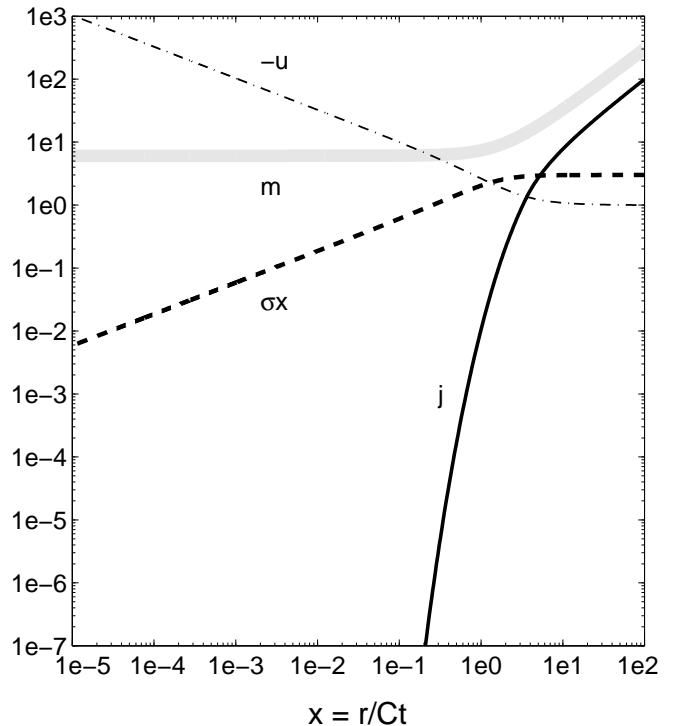


FIG. 6.— Strong-braking solution for an ideal-MHD rotational collapse. The variations of the normalized radial infall speed  $-u$ , surface density  $\sigma$ , total mass  $m$ , and specific angular momentum  $j$  are plotted as functions of the similarity variable  $x$ . Moderately fast initial rotation ( $v_0 = 1$ ) and large braking parameters ( $\alpha = \delta = 10$ ) are assumed; the other parameter values are the same as in the fiducial solution of Fig. 3. In this case  $j$  decreases to a very small value at a finite distance from the origin ( $x_j \approx 0.2$ ), and no centrifugal shock is established. The central mass is  $m_c = 6.06$ .

the central mass quoted by CCK ( $m_c = 6.1$ ) is very close to the value that we derive ( $m_c = 6.06$ ). We note, however, that the extremely rapid decrease of  $h$  with radius that is implied by this solution is unlikely to be sustained in reality. For example, when the disk becomes sufficiently thin, the radial field components on opposite sides of the disk might reconnect, resulting in an upper bound on  $b_{r,s}$ . Furthermore, the decrease in  $h$  will be arrested once the column density grows to a value for which the disk becomes opaque and the isothermal approximation breaks down. We do not consider these caveats in more detail since (as we point out at the beginning of § 3.3) we expect *radial* field diffusion to intervene (possibly even before the above effects come into play) and prevent the IMHD configuration from being set up near the center.

### 3.3. Ambipolar Diffusion-Dominated Rotational Collapse

Using the  $x \rightarrow 0$  asymptotic relations for the IMHD solution given by equations (37)–(42), it can be readily verified that the nondiffusive terms in the induction equation (22) are  $\propto x^0$  whereas the diffusive term (associated with the magnetic tension force) is  $\propto x^{-1/4}$ , so that the latter will become dominant near the origin. It follows that the IMHD solution cannot apply in the vicinity of the center in cases in which an accretion disk is predicted to form. Ambipolar diffusion must therefore be incorporated into the model, and in this subsection we describe how the nature of the solutions changes when this is done.

In the case of the asymptotic solution for a strongly braked rotational infall or a nonrotational collapse (eqs. [43]–[47]), the nondiffusive terms in equation (22) are still  $\propto x^0$ , but the dif-

diffusive term scales as  $x^{1/2}$  and remains subdominant as  $x \rightarrow 0$ . The asymptotic IMHD solution is thus self-consistent in this case, as we verified by checking that, in the model presented in Figure 6, the diffusive term is everywhere smaller than 10% of the flux-advection term (assuming  $\eta \lesssim 1$ ). This conclusion differs from that of CCK, a discrepancy that can be traced to their neglect of the magnetic squeezing term in the equation for  $h$ . However, as we noted in § 3.2.3, real disks are unlikely to become as extremely thin as the IMHD solution that incorporates this term would imply. Furthermore, the accumulation of magnetic flux at the center, which is indicated by the IMHD split-monopole solution, would lead to a severe magnetic flux problem (see § 1) if allowed to proceed and is likely prevented from occurring by the action of *Ohmic* diffusivity in the disk or the YSO (see Li & McKee 1996).

The ascendancy of the ambipolar diffusion term at low values of  $x$  means that ions and neutrals behave differently in that region. In contrast, the initial ( $x \gg 1$ ) conditions involve no field diffusivity and correspond to negligible drift between these two particle species. The study of these two regimes can be facilitated by observing that, in most cases, the strong inequality  $b_{r,s} \gg h(db_z/dx)$  is satisfied for almost all values of  $x$ : the gradient of  $b_z$  is never very large (except in shocks), and the disk is usually very thin. Under these conditions, one can treat the flux conservation relation (eq. [22]) as a quadratic equation for  $b_z$ ,

$$\eta\psi x^{-1} h^{1/2} \sigma^{-3/2} b_z^2 - x(x-u)b_z + \psi = 0, \quad (48)$$

where we regard the variables  $\psi$ ,  $h$ ,  $\sigma$ , and  $u$  as given. Equation (48) has two real roots,  $b_{z,\text{low}}$  and  $b_{z,\text{high}}$ , and we have found that in most of the solutions that we constructed they are well separated ( $b_{z,\text{low}} \ll b_{z,\text{high}}$ ). This property makes it possible to obtain simple expressions for  $b_z$  in the IMHD (large  $x$ ) and AD (small  $x$ ) regimes. Specifically, the lower root, which is applicable in the IMHD regime, can be evaluated by disregarding the quadratic term in equation (48):

$$b_{z,\text{low}} \approx \psi/xw = \sigma\psi/m. \quad (49)$$

The vertical field component in the AD regime corresponds to the larger root and can be approximated by omitting the constant term in equation (48):

$$b_{z,\text{high}} \approx \eta^{-1} x(\sigma/h)^{1/2} (m/\psi). \quad (50)$$

The transition between the IMHD and AD regimes can take place either gradually or abruptly. The latter case occurs when the flow is super-fast-magnetosonic and the flow variables are changed by passing through a shock. The occurrence of such an ambipolar diffusion-mediated shock was originally suggested by Li & McKee (1996) and subsequently verified in the nonrotating collapse calculations of CK and CCK, which succeeded in resolving the shock structure. We generalize these results to the rotating-collapse case in § 3.3.1. The most striking feature of this shock is the abrupt jump in  $b_z$  between the two roots (49) and (50) (the other flow variables are also affected, but less strongly). The jump represents a large local gradient in  $b_z$ , which implies that the term  $h(db_z/dx)$  in equation (22) can no longer be disregarded. In fact, it is this term that mediates the transition between the two roots of equation (48) and allows the shock structure to be resolved. The transition, however, remains very sharp, and equation (48) remains applicable outside a narrow neighborhood of the shock position  $x_a$ .

As in the IMHD solution presented in § 3.2, we find it convenient to distinguish between the fiducial case (§ 3.3.1) and the limiting cases of fast rotation (§ 3.3.2) and strong braking

(§ 3.3.3). In the fiducial case the braking is strong enough to place the centrifugal shock well within the AD shock ( $x_c \ll x_a$ ). The centrifugal shock again disappears in the strong-braking case, but an AD shock is still present, as in the nonrotating, diffusive solution obtained by CCK. However, in the fast-rotation case the centrifugal shock is established when the flow is still in the IMHD regime, and hence for  $x < x_c$  the inflow speed is low. In this case the transition between the IMHD and AD regimes occurs smoothly instead of in a shock (with the two roots of eq. [48] remaining close to each other), although it is still mediated by the  $h(db_z/dx)$  term in the induction equation.

To solve the self-similar equations as a boundary-value problem, it is necessary to know the asymptotic behavior for  $x \rightarrow 0$ . For a flow that continues to rotate all the way down to the origin (as in the fiducial and fast-rotation solutions), the behavior in this limit is given by

$$\dot{m} = m = m_c, \quad (51)$$

$$j = m_c^{1/2} x^{1/2}, \quad (52)$$

$$-u = w = (m_c/\sigma_1) x^{1/2}, \quad (53)$$

$$\begin{aligned} \sigma &= \frac{(2\eta/3\delta)(2m_c)^{1/2}}{[1 + (2\eta/3\delta)^{-2}]^{1/2}} x^{-3/2} \\ &\equiv \sigma_1 x^{-3/2}, \end{aligned} \quad (54)$$

$$b_z = -b_{\phi,s}/\delta = [m_c^{3/4}/(2\delta)^{1/2}] x^{-5/4}, \quad (55)$$

$$b_{r,s} = \psi/x^2 = (4/3)b_z, \quad (56)$$

$$h = \{2/[1 + (2\eta/3\delta)^2]m_c\}^{1/2} x^{3/2}. \quad (57)$$

This solution represents a Keplerian disk in which all the field components have comparable magnitudes. In contrast with the corresponding IMHD solution with its split-monopole field configuration (see eqs. [37]–[42]), in this case the field–matter decoupling brought about by the ambipolar diffusion results in a field that is not strong enough to either dilute the Keplerian rotation or to dominate the vertical compression. [The vertical squeezing of the disk in the asymptotic AD solution is dominated by the tidal and self-gravity forces, which contribute in the proportion  $1 : (2\eta/3\delta)^2$ .] The asymptotic solution in the strong-braking limit, which (as in the corresponding IMHD case) involves a flow that is nonrotating near the origin, is given in § 3.3.3.

The solutions presented in this subsection have been obtained by using the following numerical procedure:

1. Solve a simplified system of equations by disregarding the  $db_z/dx$  terms in equations (21), (22), and (31) to obtain approximate values for the five variables  $\sigma$ ,  $u$ ,  $\psi$ ,  $j$ , and  $b_z$  at a selected matching point  $x_m$ . We have found that, to assure numerical stability, it is best to choose this matching point in the region where the effects of ambipolar diffusion are just starting to become dominant.
2. Integrate the full system of equations both outward and inward from the matching point. In the outward direction, the solution reaches out to the point  $x_{\text{max}} = 10^2$ , where it must match the prescribed initial conditions of the flow (given by the parameters  $A$ ,  $u_0$ ,  $\mu_0$ , and  $v_0$ ). In the inward direction, the flow must match the  $x \rightarrow 0$  asymptotic solution (given by eqs. [51]–[57] in the fiducial and fast-rotation cases, and by eqs. [66]–[71] in the strong-braking case), which also determines the value of  $m_c$ . Except in the strong-braking limit, the flow must also incorporate a centrifugal shock (which is located

inside the matching point for the fiducial solution and outside it in the fast-rotation case). The discontinuities that some of the flow variables experience at  $x_c$  are handled using the appropriate shock jump conditions (Appendix B).

3. Iterate on the values of the five flow variables at the matching point  $x_m$  as well as on those of the central mass ( $m_c$ ) and (if applicable) of the centrifugal-shock position ( $x_c$ ) until convergence is reached.

### 3.3.1. Fiducial Solution

Our “standard” solution, corresponding to  $\eta = 1$ ,  $v_0 = 0.73$ ,  $\alpha = 0.08$ , and  $\delta = 1$ , is presented in Figure 7. In this case the initial rotation is not very fast and the braking is moderate (see § 3.2.1), so the ambipolar-diffusion shock is located further away from the center than the centrifugal shock ( $x_a/x_c \approx 30$ ). To more clearly separate the different flow regimes, we also show a solution where  $v_0$  is reduced to 0.18 (Fig. 8a), which has the effect of reducing  $x_c$  by a factor  $\sim 10$ , and another one (Fig. 8b) where, in addition,  $\eta$  is reduced to 0.7, which has the effect of further increasing  $x_a/x_c$  (to  $\sim 1 \times 10^3$ ). We now summarize the distinguishing properties of these flow regimes.

**Outer region ( $x > x_a$ ): ideal-MHD infall.** This region extends from  $x_{\max} = 10^2$ , where the initial conditions are applied, to  $x = x_a$ , the location of the resolved ambipolar diffusion shock. This region does not differ substantially from the IMHD case, with the effects of ambipolar diffusion remaining minimal. The approximation  $b_z \approx b_{z,\text{low}}$  (eq. [49]) is excellent, and it is also quite accurate to set  $\mu \equiv \sigma/b_z \approx \text{const}$ . The outer asymptotic solution remains roughly applicable for  $x \gtrsim 10$ . Although the centrifugal force is still dynamically unimportant, there is some magnetic braking, especially for  $x \lesssim 1$ , and so the ratio  $j/m$  is not exactly constant. Over most of this region the infall speed is governed by self-gravity ( $m \gg m_c$ ), but closer to the inner edge ( $x \sim 2$ ), infall starts to be dominated by the central mass.

**The ambipolar diffusion shock ( $x \approx x_a$ ).** This shock marks the end of the IMHD regime. It can be resolved as a continuous transition, although it may contain a viscous subshock. Its most notable feature is the rapid increase in  $b_z$ , which grows from essentially  $b_{z,\text{low}}$  at the outer edge of the shock transition to  $b_{z,\text{high}}$  (eq. [50]) at the inner edge. Although the inequality  $h \ll x$  continues to hold, the  $db_z/dx$  terms in the structure equations are important in this range. [It is worth noting in this connection that the sharp spike exhibited by the disk half-thickness curve at the location of the shock is a consequence of the large  $b_z$ -gradient term in eq. (31). The extreme narrowness of the spike ( $\Delta x \ll |u|h$ ) indicates, however, that the assumption of vertical hydrostatic equilibrium is not justified at that location. In reality, the enhanced magnetic squeezing at the shock will reduce the disk thickness to only a fraction of the amount indicated by the equilibrium curve over the fluid transit time through the shock. This apparent overshoot is, however, a highly localized phenomenon: the solution obtained by omitting the  $db_z/dx$  term in eq. (31) has a very similar global structure.] Immediately behind the shock the inward acceleration is temporarily reversed, resulting in a thin overshoot layer where the flow undergoes a weak outward acceleration. The shock structure is basically the same as that found in CCK for

a nonrotational flow: for our fiducial parameters, rotation is not yet dynamically significant at this location.

To obtain an estimate of the value of  $x_a$  (which can be used as an initial guess in the numerical solution), we make use of the fact that, in the infall region that is located just downstream from  $x_a$ ,  $b_{r,s} \approx b_z \approx b_{z,\text{high}}$ . These approximate equalities imply  $x^3 \approx (\eta\psi^2/m)(h/\sigma)^{1/2}$ . We evaluate this expression at  $x_a$  by using the fact that, for  $x > x_a$ , ideal MHD is approximately valid and hence  $m/\psi$  is not very different from its initial value  $\mu_0$ , and that at this location  $m$  is already close to  $m_c$  so that  $\psi \approx m_c/\mu_0 = \text{const}$ . For the solutions shown in Figures 7 and 8, the vertical squeezing at  $x_a$  is controlled by magnetic pinching, so  $h \approx 2x^4\sigma/\psi^2$  (see eq. [32]). These approximations yield an estimate of the shock location,

$$x_a \approx \sqrt{2}\eta/\mu_0, \quad (58)$$

which depends only on prespecified flow parameters. Analogous (albeit less simple) algebraic expressions can be written down for the cases in which the vertical squeezing is dominated by the central tidal force or by self-gravity.

Since the magnetic flux contained within  $x_a$  is essentially the same as the flux that initially threaded the enclosed mass, it also nearly equals the flux trapped in the central split monopole of the IMHD solution. Ambipolar diffusion does not destroy the accumulated flux but rather redistributes it between the origin and the shock location. As the value of  $x_a$  generally increases with the diffusivity parameter  $\eta$ , the approximate flux conservation within  $x_a$  implies that the vertical field component ( $\approx b_{z,\text{high}}$ ) behind the ambipolar-diffusion shock decreases with increasing  $\eta$  (in particular, it scales as  $\eta^{-2}$  when  $x_a$  is given by eq. [58]).

A comparison of Figures 8a and 8b reveals that the deceleration of the flow in the AD shock is stronger the lower the value of  $\eta$ . This can be attributed to the inferred dependence of  $b_{z,\text{high}}$  on  $\eta$ , which results in higher magnetic tension and pressure forces downstream of the shock when  $\eta$  is reduced. If  $\eta$  becomes smaller than  $\sim 0.2$  (with the other parameters remaining unchanged), then the localized decrease of the infall speed inward of  $x_a$  becomes large enough to reduce  $w \equiv x - u$  below 1. But  $w = 1$  is the singular line of the AD system of equations, corresponding to the critical (sonic) speed (see Appendix B). A crossing of this curve signals a discontinuity in the flow parameters, which in this case implies the presence of an unresolved viscous subshock at the downstream end of the resolved MHD shock transition (see Li 1998).

**AD-dominated infall ( $x_c < x < x_a$ ).** Over most of the region between the two shocks the centrifugal force remains dynamically unimportant, so matter moves almost in free fall, with the gravitational force dominated by the central mass. The ions and field are only weakly coupled to the neutrals, with the ion radial speed being effectively zero (except in the vicinity of  $x_c$ ). The vertical field component continues to be given by  $b_z \approx b_{z,\text{high}}$  to a very good approximation. In many respects this zone resembles the innermost region of the nonrotating flow studied by CCK, especially when it is fairly extended ( $x_a \gg x_c$ ), as it is in the two solutions presented in Figure 8. In particular,  $b_z \propto x^{-1}$ ,  $\psi \approx x^2 b_z$ , and (over a somewhat narrower range)  $\sigma \propto w \propto x^{-1/2}$ . If this region is wide enough, magnetic braking can reduce  $j$  to an essentially constant value,  $j \approx j_{\text{pl}}$ . The mass is also well approximated by its plateau value (see eq. [35]),  $m \approx m_{\text{pl}} \approx m_c$ .

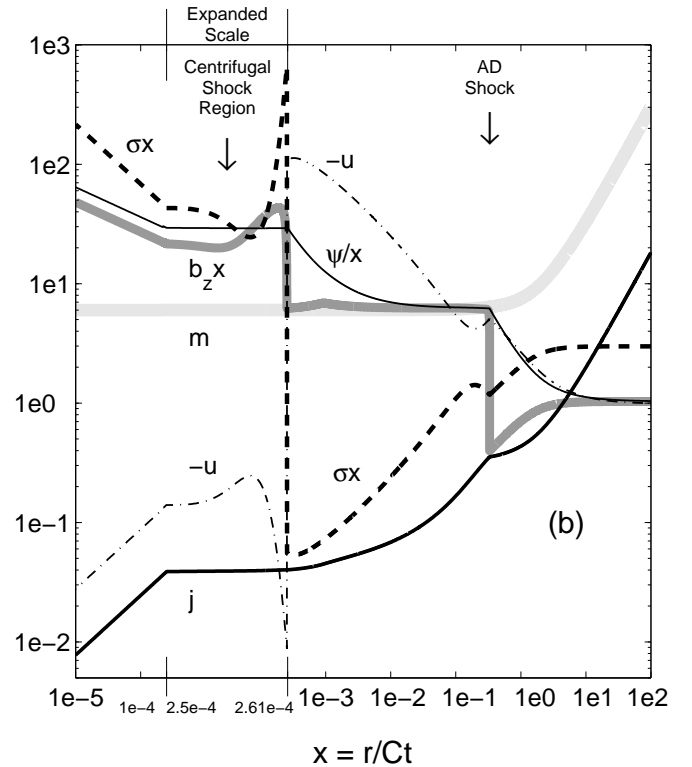
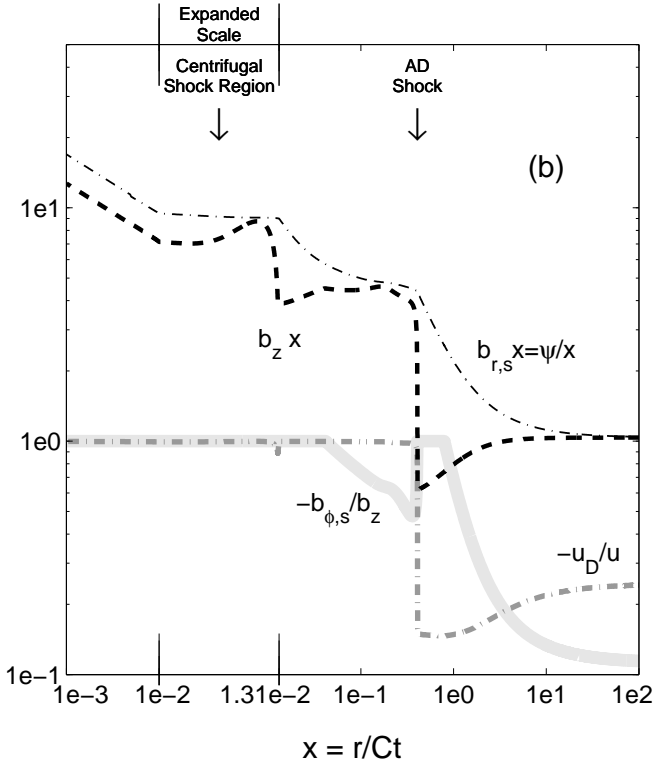
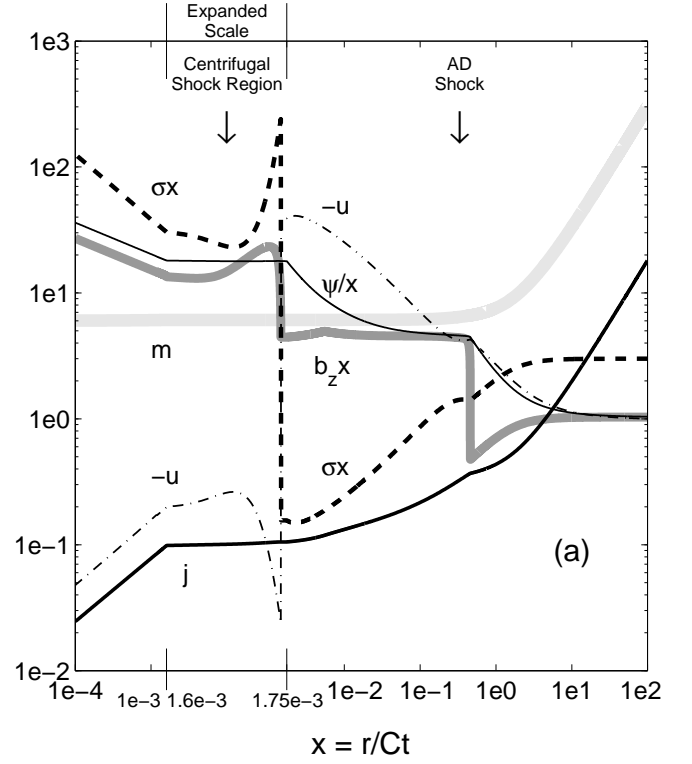
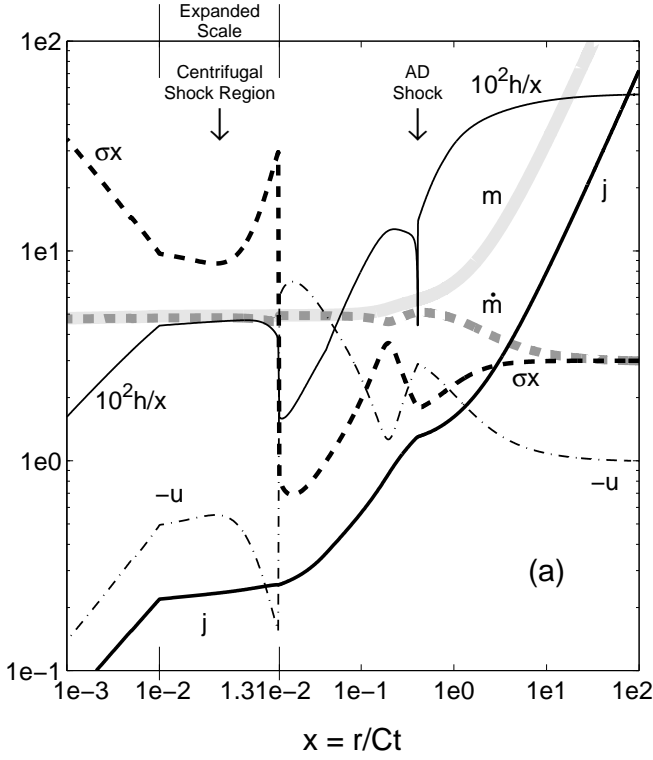


FIG. 7.— Fiducial solution for an ambipolar-diffusion rotational collapse. The variations of the normalized radial infall speed  $-u$ , surface density  $\sigma$ , total mass  $m$ , mass accretion rate  $\dot{m}$ , specific angular momentum  $j$ , and the disk half-thickness  $h$  as functions of the similarity variable  $x$  are plotted in Fig. 7a, and the corresponding variations of the  $z$  component ( $b_z$ ) and the surface radial ( $b_{r,s} = \psi/x^2$ ) and azimuthal ( $b_{\phi,s}$ ) components of the magnetic field, as well as of the normalized radial component of the ion-neutral drift velocity ( $u_D \equiv V_{D,r}/C$ ), are shown in Fig. 7b. The diffusivity parameter is  $\eta = 1$ . The other parameter values are  $v_0 = 0.73$ ,  $A = 3$ ,  $u_0 = -1$ ,  $\mu_0 = 2.9$ ,  $\alpha = 0.08$ , and  $\delta = 1$ . The ambipolar-diffusion and centrifugal shocks are located at  $x_a = 0.41$  and  $x_c = 1.3 \times 10^{-2}$ , respectively. The central mass is  $m_c = 4.7$ , and the plateau values in the AD-dominated infall region are  $m_{pl} \approx 4.9$  and  $j_{pl} \approx 0.26$ .

FIG. 8.— (a) Same parameter values as in Fig. 7, except that  $v_0$  is reduced from 0.73 to 0.18. In this case  $x_a = 0.46$ ,  $x_c = 1.7 \times 10^{-3}$ ,  $m_c = 6.0$ ,  $m_{pl} = 6.1$ , and  $j_{pl} \approx 0.1$ . (b) Same as Fig. 8a, except that the diffusivity parameter  $\eta$  is reduced from 1 to 0.7. In this case  $x_a = 0.33$ ,  $x_c = 2.6 \times 10^{-4}$ ,  $m_c = 6.00$ ,  $m_{pl} = 6.03$ , and  $j_{pl} \approx 0.04$ . The horizontal scale in the vicinity of the centrifugal shock has been expanded to show details of the postshock transition zone.

As we point out in § 4,  $m_c$  will be reduced below the value of  $m$  upstream of the centrifugal shock if (as expected) the rotationally supported disk drives a wind from its surfaces. The numerical value of the reduction factor depends, however, on yet another model parameter (see eq. [C6]). Therefore, to simplify the discussion, we have chosen not to incorporate the effect of the wind mass loss into the solutions that we present.

The centrifugal force starts to become important near the downstream end of this zone: after it comes to exceed the gravitational force, it triggers the formation of the centrifugal shock at the point  $x_c \approx j_{\text{pl}}^2/m_c$ . In contrast to the IMHD solution presented in § 3.2.1, one cannot approximate  $j_{\text{pl}}$  by its initial value in this case: the braking action induced by the magnetic field amplification in the AD shock completely invalidates this approximation. A comparison of Figures 8a and 8b illustrates this point. When  $\eta$  is reduced from 1 (Fig. 8a) to 0.7 (Fig. 8b), the location of the AD shock changes by a factor of  $\sim 0.7$  and the value of the central mass remains essentially the same: this is as expected from equations (58) and (35), respectively. However, the decrease in  $\eta$  has a very pronounced effect on the location of the centrifugal shock: as  $\eta$  is reduced by a factor of  $\sim 1.4$ ,  $x_c$  decreases by a factor of  $\sim 6.7$ . As we now demonstrate, this can be traced to the sensitive dependence of the magnetic braking term on  $\eta$ , which leads to a strong reduction in  $j$  downstream from the AD shock for even a moderate decrease in  $\eta$ .

We first estimate  $b_{\phi,s}$  by substituting  $b_z$  from equation (50) into equation (24) and using equation (25),

$$b_{\phi,s} \approx -2\alpha\psi jx^{-3}(1+2\alpha w)^{-1}. \quad (59)$$

Equation (23) then yields

$$\frac{dj}{dx} \approx -(x^2/m)b_z b_{\phi,s} \quad (60)$$

$$\approx 2\alpha\eta^{-1}j(\sigma/h)^{1/2}(1+2\alpha w)^{-1}. \quad (61)$$

Using again the approximations  $b_{r,s} \approx b_z$  and  $h \approx 2\sigma/b_{r,s}^2$  that were employed in deriving the above estimate of  $x_a$ , equation (61) becomes

$$\frac{dj}{dx} \approx \frac{\alpha m}{\eta^2 x} j(1+2\alpha w)^{-1}. \quad (62)$$

Using the approximations  $w \approx (2m/x)^{1/2}$  and  $m \approx m_c$ , and assuming that  $2\alpha w \gg 1$ , we get

$$\frac{dj}{dx} \approx (m_c/8)^{1/2}\eta^{-2}x^{-1/2}j. \quad (63)$$

This equation can be integrated to give

$$j = j_1 \exp\left\{(m_c/2)^{1/2}\eta^{-2}x^{1/2}\right\}, \quad (64)$$

where  $j_1$  is a constant. This result is valid between  $x_a$  and  $x_c$  and can be used to estimate the latter. For  $x_c \ll x_a$ , the value of  $j$  at  $x_c$  may be identified with  $j_{\text{pl}}$  and can be approximated by  $j_1$ . Assuming also that no significant magnetic braking takes place for  $x > x_a$  (consistent with our analysis of the IMHD solution in § 3.2.1), we can write  $j_{\text{pl}} \approx (v_0/A)m_{\text{pl}} \approx (v_0/A)m_c$ . Using equation (58) to evaluate  $x_a$ , we finally obtain

$$x_c \approx \frac{v_0^2}{A^2}m_c \exp\left\{-(2^{3/2}\eta^{-3}m_c/\mu_0)^{1/2}\right\}. \quad (65)$$

We have verified that this estimate (which depends on the ratio  $x_a/x_c$  being  $\gg 1$ ) yields the value of  $x_c$  to within 30% for both of the solutions shown in Figure 8. The strong dependence of  $x_c$  on  $\eta$  that is exhibited by these solutions can be understood from the form of the expression (65): it indicates that the effect of even a small variation in  $\eta$  is magnified on account of

its presence inside an exponential function. Although the precise form of this expression may be expected to differ in cases where some of the approximations we utilized do not apply, the sensitive dependence of  $x_c$  on  $\eta$  is probably a general feature of the model.

**The centrifugal shock ( $x \approx x_c$ ).** The shock represents a discontinuity in the variables  $u$ ,  $\sigma$ , and  $b_z$  through which the flow changes from the nearly undiluted free fall to subsonic accretion. We approximate the shock as a discontinuity in the variables  $u$  and  $\sigma$ , which is governed by the isothermal-shock jump conditions (Appendix B.1), followed by a very thin (but numerically resolvable) layer where  $b_z$  increases. In this picture, the ions are decoupled from the neutrals inside the subshock, so their radial speed in the frame of the shock, and hence (by magnetic flux conservation, see eq. [A18])  $B_z$ , remain unchanged across the subshock even as  $|V_r|$  and  $\Sigma$  vary. However, the increase in the drift speed  $|V_{D,r}|$  across the subshock enhances the collisional drag force immediately behind it and causes a local recoupling of ions and neutrals; this, in turn, leads to a rapid decline in  $|V_{i,r}|$  and a consequent increase in  $B_z$ . Just inward of the shock there is a narrow transition zone where the flow settles down to its asymptotic Keplerian structure. Within this layer the variables  $u$ ,  $\sigma$ , and  $b_z$  adjust rapidly (with some oscillations and overshoots) to their asymptotic values. This implies, in particular, that, just as in the case of the AD shock, the derivative terms  $hdb_z/dx$  in the constituent equations cannot be neglected in this zone. The surface density in this region is significantly larger than  $\sigma$  in its immediate vicinity, so the layer represents a massive ring lying just outside the main body of the disk (resembling the situation in the fiducial IMHD solution considered in § 3.2.1). In the solution shown in Figure 7, the width of the ring is  $\sim 10\%$  of  $x_c$  and it encompasses  $\sim 8\%$  of the total mass of the disk within  $x_c$ ; the relative size of the ring in the solutions displayed in Figure 8 is, however, smaller. The variables  $\psi$  and  $j$  do not change appreciably across this region.

**The Keplerian disk ( $x < x_c$ ).** Inward of the postshock transition layer, the flow approaches the form of a magnetized Keplerian accretion disk as described by equations (51)–(57). For the solutions shown in Figures 7, 8a, and 8b, the total mass of the rotationally supported disk (including the ring at  $x_c$ ) is, respectively,  $\sim 5\%$ ,  $\sim 2\%$ , and  $\sim 0.4\%$  of  $m_c$ .

### 3.3.2. Fast Rotation

As in the corresponding IMHD case, a high value of  $v_0$  and comparatively low values of  $\alpha$  and  $\delta$  result in the centrifugal shock being located within the self-gravity-dominated region (where  $m \gg m_c$ ). The value of  $x_c$  is large enough for ideal MHD to still be applicable (so  $\psi \approx xwb_z$ ). Since the inflow speed is strongly reduced in the dense disk that forms behind the centrifugal shock, the ambipolar-diffusion time becomes shorter than the accretion time and an AD transition front is established not far from  $x_c$ . In fact, as  $-u$  is small enough for the flow to remain subsonic ( $x - u < 1$ ) in this region, the IMHD-to-AD transition is gradual rather than sharp as in the other cases considered in this subsection, where it takes the form of an AD shock. Since the centrifugal shock occurs within the ideal-MHD region, we impose the same jump conditions at  $x_c$  as in the corresponding IMHD case (see § B.2).

A representative solution is shown in Figure 9. It exhibits the same general features (a non-Keplerian outer region, a small

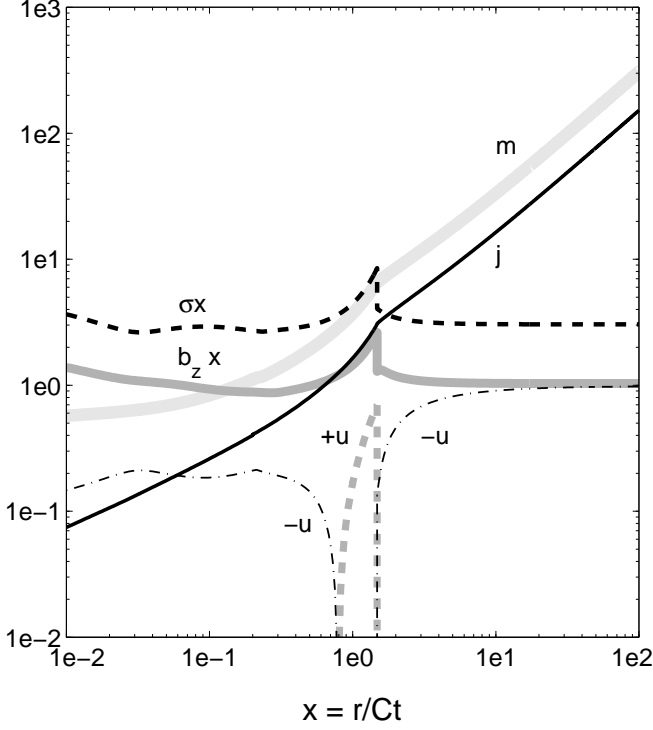


FIG. 9.— Fast-rotation solution for an ambipolar-diffusion rotational collapse. The variations of the normalized radial infall speed  $-u$ , surface density  $\sigma$ , total mass  $m$ , specific angular momentum  $j$ , and  $z$  component of the magnetic field  $b_z$  are plotted as functions of the similarity variable  $x$ . The model parameter values are the same as in the fiducial case (Fig. 7), except that the azimuthal-velocity parameter  $v_0$  is increased from 0.73 to 1.5 and the braking parameter  $\alpha$  is increased from 0.08 to 0.1 (so they match the corresponding parameters in the ideal-MHD solution depicted in Fig. 4). The derived values of the centrifugal-shock radius ( $x_c = 1.5$ ) and of the central mass ( $m_c = 0.5$ ) are similar to those of the corresponding ideal-MHD solution.

central mass, a backflowing layer behind the centrifugal shock) as the fast-rotation IMHD solution (see Figs. 4 and 5). These characteristics are basically a consequence of the fast initial rotation, and the strong similarity with the corresponding IMHD case shown in Figure 4 can be understood from the fact that the centrifugal shock occurs outside the AD regime.

### 3.3.3. Strong Braking

In § 3.2.3 we have found that ideal-MHD flows with strong braking can lose all their angular momentum at a finite distance from the origin. Here we consider whether a similar situation can occur in the presence of ambipolar diffusion.

When  $j = 0$  there are two inner asymptotic solutions that are mathematically self-consistent and that can be matched to the outer asymptotic solution by integrating the system of differential equations. Correspondingly, two kinds of solutions are found: one that is almost IMHD in nature, and another that is AD dominated.

The IMHD-like solution resembles the one obtained in § 3.2.3 in that  $b_z$  is everywhere well approximated by the root  $b_{z,\text{low}}$  of equation (48), there is no AD shock, and the inner asymptotic solution is given by equations (43)–(47) (but with  $\mu$  possibly differing from  $\mu_0$  on account of the small, but finite, ambipolar diffusion). Outside the point  $x_j$  the azimuthal field component can differ significantly from its IMHD value, but once complete braking is accomplished and both  $v$  and  $b_{\phi,s}$  effectively vanish, this solution basically describes an IMHD nonrotating inflow and, in particular, predicts the formation of

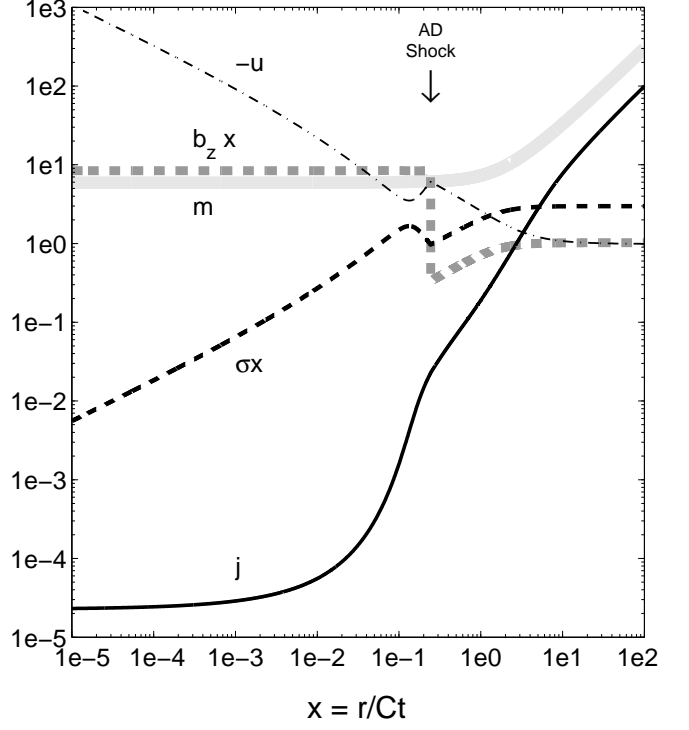


FIG. 10.— Strong-braking solution for an ambipolar-diffusion rotational collapse. The variations of the normalized radial infall speed  $-u$ , surface density  $\sigma$ , total mass  $m$ , specific angular momentum  $j$ , and  $z$  component of the magnetic field are plotted as functions of the similarity variable  $x$ . The model parameters are  $\eta = 0.5$ ,  $v_0 = 1$ ,  $\alpha = 10$ , and  $\delta = 10$ , with the remainder having the same values as in the fiducial case (Fig. 7). Note that  $j$  attains a tiny, but finite, plateau value in the innermost (free-fall) region ( $j_{\text{pl}} = 2 \times 10^{-5}$ ). The AD shock is located at  $x_a = 0.24$ , and the central mass is  $m_c = 5.9$ .

a central split-monopole field. As we remarked at the beginning of § 3.3, such a configuration is unlikely to occur in real systems, so we henceforth concentrate on the more plausible alternative case.

In the diffusive solution, the flow passes through an AD shock at a point  $x_a$  (which can be estimated by eq. [58]) that typically exceeds  $x_j$ . Inward of the ambipolar-diffusion shock, the poloidal field components have the same form as in the fiducial solutions,  $b_{r,s} \approx b_z \approx b_{z,\text{high}}$ . As in the corresponding IMHD case, the inner asymptotic solution satisfies  $j = b_{\phi,s} \approx 0$  and describes a free fall onto the central mass, which, however, in this case is *not* magnetically diluted but rather resembles the situation in the AD-dominated infall region of the fiducial solutions. It is given by

$$\dot{m} = m = m_c, \quad (66)$$

$$-u = (2m_c/x)^{1/2}, \quad (67)$$

$$\sigma = (m_c/2x)^{1/2}, \quad (68)$$

$$b_z = 2^{-1/8} m_c^{5/8} \eta^{-1/2} \tilde{h}^{-1/4} x^{-1}, \quad (69)$$

$$b_{r,s} = \psi/x^2 = b_z, \quad (70)$$

$$h = \tilde{h} x^{3/2}. \quad (71)$$

The power-law scalings of the flow variables with  $x$  are the same as in the asymptotic solution obtained by CCK for the nonrotating AD collapse. However, because of the magnetic pinching effect included in the above solution, the expression

for the coefficient  $\tilde{h}$  is more involved:

$$\tilde{h} = \left[ \frac{(12D/\sqrt{G} - G)^{1/2} - \sqrt{G}}{2\sqrt[3]{6}} \right]^2, \quad (72)$$

$$D = N^{1/4}/\eta, \quad (73)$$

$$N = 2/m_c, \quad (74)$$

$$G = (2F)^{1/3} - 8N(3/F)^{1/3}, \quad (75)$$

$$F = 9D^2 + [3(27D^4 + 256N^3)]^{1/2}, \quad (76)$$

with the expression for  $\tilde{h}$  representing the real, positive solution of the quartic equation  $\tilde{h}^2 + D\tilde{h}^{1/2} - N = 0$ .

An example of a strongly braked solution is shown in Figure 10. A curious feature of the flow is the value of  $j$  as  $x \rightarrow 0$ , which assumes a nonzero (albeit rather small) plateau value ( $j_{\text{pl}} \sim 10^{-5}$ ). This puzzling behavior can be attributed to the very small magnitude of  $\psi$  in this limit, which causes  $|b_{\phi,s}|$  (eq. [24]) and therefore  $|dj/dx|$  (eq. [23]) to be small, more than compensating for the increase in  $b_z$  behind the AD shock. The low value of the angular-momentum derivative in turn accounts for the asymptotic near-flatness of the  $j$  curve. (In contrast, the large central value of  $\psi$  associated with the split-monopole field in the near-IMHD solution guarantees that, in this case,  $|b_{\phi,s}|$  and  $|dj/dx|$  remain large enough near  $x_j$  to make  $j$  actually vanish there.) The value of  $j_{\text{pl}}$  is highly sensitive to the magnitude of the parameter  $\eta$ : it decreases by  $\sim 10$  orders of magnitude when  $\eta$  is decreased from 0.5 to 0.3. (The strong sensitivity of  $x_c$  to the value of this parameter has already been noted in connection with the fiducial solutions; see eq. [65].) However, for practical purposes,  $j_{\text{pl}}$  can be regarded as being effectively zero. In particular, the implied location of the centrifugal radius,  $x_c \approx j_{\text{pl}}^2/m_c$ , corresponds to such a small radius for any meaningful value of  $t$  that it would invariably lie well inside the central protostar.

#### 4. DISCUSSION

The model presented in this paper provides a physical framework for a detailed study of the development of star-disk systems in the collapse of rotating, magnetic molecular-cloud cores. Perhaps the most noteworthy feature of the solutions presented in § 3 is that, for representative values of the initial cloud rotation and magnetization and with plausible estimates of the magnetic field diffusivity and of the strength of magnetic braking, they predict the formation of circumstellar disks whose properties compare quite well with those of real protostellar systems. In particular, the disks obtained for our chosen fiducial parameters are *Keplerian*, having a mass that is only a small fraction ( $\lesssim 10\%$ ) of the central mass, as has been inferred for most protostellar disks in nearby dark clouds (see § 2.1). For the representative AD solution shown in Figure 7 (corresponding to  $\eta = 1$ ,  $v_0 = 0.73$ ,  $\alpha = 0.08$ , and  $\delta = 1$ ), the disk mass  $M_d$  is less than 5% of the central mass  $M_c$ . For comparison, if the model parameters are slightly changed (to  $\eta = 1$ ,  $v_0 = 0.77$ ,  $\alpha = 0.11$ , and  $\delta = 0.7$ ), one finds  $M_d/M_c \approx 9\%$ . The most reliable protostellar disk velocity curves have been obtained in Class II YSOs (i.e., T Tauri stars, of typical ages  $\sim 10^6$  yr), which, in contrast to younger protostars, are no longer strongly obscured by dusty envelopes (identified with the contracting cloud cores). These are also the systems with the most accurate determinations of the disk mass (e.g., Mundy et al. 2000): the massive envelopes surrounding Class 0 YSOs prevent their disk masses from being pinned down, and even in the case of Class I sources the values

of  $M_d$  are not as well determined (although they appear to be similar to the disk masses in Class II systems). It has occasionally been suggested in the literature that protostellar disks may not be Keplerian during the early (in particular, Class-0) phase of their evolution, when the ratio of the central mass to that of the surrounding envelope is still small. Our results demonstrate that this need not be the case. In fact, in the self-similar solutions that we derive, if the mass of the rotationally supported disk is small in comparison with the central mass at any given time, it will be so at all times.

The observed rotationally supported disks typically have sizes  $\lesssim 10^2$  AU (see § 1), which are reproduced by our typical solutions. For example, the derived disk size (given by the value of the centrifugal radius  $r_c$ )  $10^5$  yr after the start of the collapse (which corresponds to the Class-I evolutionary phase) is  $\sim 52$  AU for the fiducial solution presented in Figure 7 and  $\sim 130$  AU for the other AD solution mentioned in the preceding paragraph. There have been reports in the literature of T Tauri circumstellar disks that exhibit Keplerian rotation on somewhat larger scales [e.g., GM Aur, with  $r_c > 200$  AU (Dutrey et al. 1998), and DM Tau, with  $r_c > 600$  AU (Guilloteau & Dutrey 1998)]. It is quite possible that these disks have achieved their large sizes already during their early evolutionary stages. For example, they may have possessed a comparatively high value of the diffusivity parameter  $\eta$ , to which the predicted magnitude of  $r_c$  is particularly sensitive (see eq. [65]). Alternatively, they may have formed from collapsing cores with comparatively large initial rotations and relatively inefficient braking (see § 3.3.2). It is worth noting, though, that in the self-similar model, disks with larger values of  $x_c$  tend to have higher disk-to-star mass ratios and therefore exhibit progressively greater departures from a Keplerian rotation law. It is, however, also conceivable that at least part of the cause for large observed disk sizes in these highly evolved (and no longer strongly accreting) systems is post-formation viscous spreading of the disk (e.g., Lin & Pringle 1990; Hartmann et al. 1998). It is interesting to note in this connection that the radial scaling of the disk surface density predicted by our self-similar solution ( $\Sigma \propto r^{-3/2}$  for small  $r$ ; see eq. [54]) is the same as that inferred for the “minimum mass” solar nebula (Weidenschilling 1977; Hayashi, Nakazawa, & Nakagawa 1985). Although this agreement is encouraging, it is not unique to this model: in particular, the same scaling is predicted for a self-similar *Keplerian* disk with “ $\alpha$  viscosity” (Tsuribe 1999) and for a self-similar *self-gravitating* disk with a gravitational instability-induced effective viscosity (Lin & Pringle 1987).

Our model disks exhibit a surface-density enhancement near their outer edges (see § 3.2.1 and § 3.3.1): for the fiducial AD solution shown in Figure 7, this ring has a mass  $\sim 0.1 M_d$  and a width  $\sim 0.13 r_c$ . We are not aware of any observational evidence as yet for the existence of such rings in protostellar systems, but there have been several recent reports of well-defined dust rings with similar radii ( $\sim 10^2$  AU) and fractional widths around older, Vega-like stars (e.g., Schneider et al. 1999; Dent et al. 2000; Koerner, Sargent, & Ostroff 2001). Although the apparent confinement of the latter rings is usually attributed to the presence of solid “satellites” (e.g., planets), it is interesting to speculate that their origin could be traced to the  $\Sigma$  enhancements predicted by our solutions.

An important implication of the result that typical rotating inflows tend to produce a central mass that is surrounded by a Keplerian disk is that the angular momentum problem (see



§ 1) for the modeled YSO is basically resolved. In particular, angular momentum transport can be sufficiently efficient to allow most of the inflowing mass to end up (with effectively no angular momentum) at the center, with the central mass dominating the dynamics well beyond the outer edge of the disk even as the inflow is still in progress. Our solutions reveal that the AD shock, even though it is usually located well outside the region where the centrifugal force becomes important, helps to enhance the efficiency of angular momentum transport through the magnetic field amplification that it induces. In practice, the ultimate value of the protostellar angular momentum would be determined by the braking mechanism that enables the YSO to reduce its angular velocity below the centrifugal-equilibrium value that characterizes the accreted disk matter (e.g., Mestel & Spruit 1987; Königl 1991; Popham 1996).

The formation of Keplerian circumstellar disks in our “standard” solutions is a consequence of efficient magnetic braking, which allows the mass injected at large distances to reach the center rather than pile up in the disk (as it does in the fast-rotation solutions discussed in § 3.2.2 and § 3.3.2). The disk in these cases therefore has little influence on the mass accretion rate onto the central YSO,  $\dot{M}_c = 1.59 \times 10^{-6} (T/10\text{K})^{3/2} m_c M_\odot \text{yr}^{-1}$ , which is determined on scales much larger than  $r_c$ . In fact, as we discuss in § 3.1, the eigenvalue  $m_c$  is typically also insensitive to the magnetic structure of the flow and is often well approximated by the “plateau” value  $m_{\text{pl}}$  (eq. [35]) that depends only on the initial conditions. (For our fiducial parameters,  $m_{\text{pl}} = 6$ , implying  $\dot{M}_c \approx 9.5 \times 10^{-6} M_\odot \text{yr}^{-1}$ .) The likely production of a centrifugally driven wind that transports mass away from the disk surfaces (see discussion below) will, however, act to reduce the value of  $m_c$ : as we estimate in Appendix C, the reduction factor could be as large as  $\sim 3$ .

The presence of rotation also does not strongly affect the “revitalization” of ambipolar diffusion behind the AD shock, which, as we noted in § 1, can go a long way toward resolving the magnetic flux problem. This conclusion applies even in the fast-rotation case (see § 3.3.2), where the AD shock is replaced by a more gradual transition occurring within the disk. The asymptotic  $x \rightarrow 0$  similarity solution for the disk implies that, at any given time, the magnetic flux scales as  $r^{3/4}$  (see eq. [56]), which represents a slower decrease with  $r$  than in the nonrotating case (in which  $\Psi \propto r$ ; see eq. [70]). However, in reality, the amount of magnetic flux that ends up threading the protostar would depend on the detailed flux transport and destruction mechanisms that operate in the inner disk and the star, which may involve Ohmic resistivity (e.g., Li & McKee 1996), ambipolar diffusion (e.g., Desch & Mouschovias 2001), and reconnection (e.g., Goodson & Winglee 1999).

The quasi-equilibrium disk configurations described by our solutions make it possible to investigate the stability properties of the modeled circumstellar disks. Although a full pursuit of this topic is beyond the scope of this paper, we comment briefly on the basic MHD and gravitational instabilities that may affect the disks. The most relevant MHD instability is evidently the magnetorotational one, which is expected to develop rapidly in any differentially rotating disk that is threaded by a subthermal magnetic field (see Balbus & Hawley 1998 for a review). This instability has been shown to generate turbulence that can remove angular momentum from the inflowing gas, so the determination of whether the disk is susceptible to this instability also has implications to the self-consistency of our identifica-

tion of magnetic braking as the dominant angular-momentum transport mechanism in the disk.

As it turns out, our diffusive Keplerian disk models are by and large magnetorotationally *stable*. Physically, this is because the coupling between the matter and the field is generally too weak to allow the instability to grow. Specifically, a necessary condition for this instability to operate in a weakly ionized, Keplerian disk is  $\tau_{\text{ni}} < \Omega_K^{-1}$ , where  $\Omega_K$  is the Keplerian angular velocity (Blaes & Balbus 1994). Using our self-similar variables, this criterion can be written as  $(\sigma x^3 / m_c h \eta^2)^{1/2} > 1$ . Since the Keplerian disk region in all of our typical solutions nearly coincides with the region where the inner asymptotic solution (eqs. [51]–[57]) is applicable, we can use the latter to evaluate the left-hand side of the above inequality; it is found to equal  $2/3\delta$ . [The asymptotic solution satisfies the weak-field condition  $V_{Az}^2/C^2 < 1$  postulated in the derivation of the instability criterion; indeed, the left-hand side of the latter inequality (which equals  $b_z^2 h / \sigma$ ) vanishes ( $\propto x^{1/2}$ ) as  $x \rightarrow 0$ .] But the parameter  $\delta$  (defined in § 2.1) is expected to be  $\gtrsim 1$ , and therefore the instability condition  $\tau_{\text{ni}} \Omega_K < 1$  is not satisfied. Interestingly, our fiducial IMHD solution is also magnetorotationally stable. In this case the strong magnetic squeezing prevents the unstable perturbations from fitting inside the disk. Formally, one requires the critical wavelength  $\lambda_c \approx 3.6(V_{Az}/\Omega_K)$  to be less than the disk thickness  $2H$  for the disk to be unstable. Using the inner asymptotic solution given by equations (37)–(42), with the help of which we first verify that  $V_{Az}^2/C^2$  again tends to zero as  $x \rightarrow 0$ , this condition translates into  $1.8(m_c/2\mu^4 x)^{1/2} < 1$ . For our typical parameters this requires  $x \gtrsim 0.14$ , but this lower bound exceeds  $x_c$  (the approximate disk outer boundary) for this solution.

The above results support the choice of magnetic braking as the main angular momentum transport mechanism in our disk model. This mechanism remains effective even in the presence of ambipolar diffusion because the neutral-ion collision time  $\tau_{\text{ni}}$ , while being comparatively long, is shorter than the magnetic braking time  $\tau_{\text{br}}$ . In a Keplerian accretion disk  $\tau_{\text{br}} \approx r/|V_r|$  and  $V_r$  is typically much smaller than the Keplerian speed; therefore  $\tau_{\text{ni}}/\tau_{\text{br}}$  can be  $\ll 1$  even if  $\tau_{\text{ni}}\Omega_K$  exceeds 1. This conclusion continues to hold when the angular momentum transport in the disk (and hence the accretion time  $r/|V_r|$ ) is controlled by a centrifugally driven wind rather than by the propagation of torsional Alfvén waves. As we show in Appendix C, the basic formalism of our model is unchanged in this case, and the parameter  $\delta$  (which is now determined directly from the centrifugal wind solution) is again typically small enough for the linear stability criterion  $\tau_{\text{ni}}\Omega_K > 1$  to be satisfied over most of the disk column density. The argument against instability is reinforced by indications from numerical simulations (e.g., Hawley & Stone 1998) that MRI-driven turbulence and the resulting angular-momentum transport are significant only when  $\tau_{\text{ni}}\Omega_K \ll 1$ . We note in this connection that even a disk in which the bulk of the material is weakly coupled is expected to possess well coupled ( $\tau_{\text{ni}}\Omega_K < 1$ ) surface layers from which the centrifugal wind is launched (see Appendix C). It is, however, likely that the critical wavelength for instability exceeds the density scale height in the strongly coupled regions (see Wardle & Königl 1993 and Li 1996), so the surface layers should typically also be magnetorotationally stable.

The basic gravitational instability that we consider involves fragmentation induced by the disk self-gravity. The relevant stability condition against axisymmetric perturbations is

given by the Toomre criterion  $Q_{\text{Toomre}} \equiv C\kappa/\pi G\Sigma > 1$  (Toomre 1964), where  $\kappa = [r^{-3}(dJ^2/dr)]^{1/2}$  is the epicyclic frequency. Although this criterion is modified somewhat by magnetic effects (Shu & Li 1997; R. Krasnopolsky & A. Königl, in preparation), the corrections remain small for nearly Keplerian disks, especially in the AD regime, and we therefore neglect them here. We have verified that the Toomre criterion is well satisfied for most of our rotationally supported disk solutions, the only exceptions being the outermost (backflow) regions of the fast-rotation configurations (Figs. 4, 5, and 9), where the effect of self-gravity is comparatively large. This result is significant in that it suggests that in typical cases protostellar disks may not fragment even during the early phases of their evolution, when the central mass is still small. In our model this behavior can be attributed to the fact that, for representative parameters, the central gravity already dominates at the location of the centrifugal shock, so that the disks are nearly Keplerian from the start. Inasmuch as the inequality  $Q_{\text{Toomre}} \lesssim 1$  signals the onset of self-gravity-induced angular-momentum transport in the disk (e.g., Lin & Pringle 1987), this result also serves to justify the neglect of such a transport mechanism in our model. We note, however, that the collapsing core could in principle be unstable to fragmentation before point-mass formation, or, following PMF, in the region outside the rotationally supported disk (e.g., Boss 2000). It is also conceivable that fragmentation might be initiated even before a dynamically unstable core is formed (possibly triggered by an AD-mediated instability in the magnetically supported parent cloud; see Zweibel 1998 and Indebetouw & Zweibel 2000).

Another potential angular-momentum transport mechanism that was not included in our model involves centrifugally driven disk outflows. For a cold, thin, Keplerian disk that is threaded by open magnetic field lines, such an outflow could be launched if the angle between the meridional projection of the magnetic field and the rotation axis exceeds  $30^\circ$  (Blandford & Payne 1982). This condition is satisfied by our asymptotic disk solutions — in particular, the AD inner asymptotic solution implies a radially constant inclination angle  $\sim 53^\circ$  (see eq. [56])— so our model disks can be expected to give rise to outflows of this type. This result is encouraging in view of the fact that centrifugally driven disk outflows are a leading candidate for the origin of the bipolar outflows that are frequently observed to emanate from YSOs (see, e.g., Königl & Pudritz 2000 for a review). A centrifugally driven disk outflow can be incorporated into our model by taking account of the fact that the wind would be quasi-steady on the accretion time scale and should thus be well approximated by a steady-state formulation. The condition that the centrifugal outflow control the vertical angular momentum transport from the disk is equivalent to the requirement that the steady-state wind solution pass through the Alfvén critical point. This requirement, in turn, serves to fix the value of  $B_{\phi,s}$  (or, equivalently, of the parameter  $\delta$ ) in the disk solution. Besides angular momentum, the wind also carries away mass, resulting in a progressive decline in the mass accretion rate with decreasing disk radius and leading to lower values of  $\dot{m}$  and  $m$  at the center. Interestingly, the radial scaling of the disk magnetic field ( $\propto r^{-5/4}$ ; see eq. [55]) implied by the asymptotic AD disk solution for any given value of  $t$  is the same as in the Blandford & Payne (1982) radially self-similar, steady-state wind solution. This suggests that the latter solution can be used in conjunction with our disk model to fix the values of  $\delta$  and of the  $m_c$  reduction factor in the asymptotic disk

solution. We discuss the implementation of this scheme in Appendix C. Inasmuch as the incorporation of a disk wind does not qualitatively change our basic results, we have not included its effects in the model described in § 2 so as not to unduly complicate the presentation. It is nevertheless important to recognize that our solutions indicate that the collapse of rotating, magnetic cloud cores naturally gives rise to disks with magnetic field configurations that are conducive to the launching of centrifugally driven winds. This conclusion is supported by the MHD core-collapse numerical simulations of Tomisaka (1998, 2000, 2002), in which disk outflows that transport angular momentum through material and magnetic stresses are observed to form. (The possibility that a disk formed in the collapse of a magnetized rotating cloud core could give rise to a centrifugally driven wind was recognized also by Contopoulos & Sauty (2001). However, in contrast with our model, in their picture the angular momentum transport in the disk is dominated by turbulent viscosity and the outflow is concentrated near the outer disk radius; furthermore, they infer that the mass outflow rate depends sensitively on the efficiency of magnetic braking in the precollapse core.)

We have also presented solutions (§ 3.2.3 and § 3.3.3) in which the magnetic braking is sufficiently efficient to prevent the formation of a rotationally supported disk from the collapse of a rotating cloud core. Although we argued that the parameter combinations characterizing these solutions are not typical, it is conceivable that such situations could be realized. A possible indication that this may sometimes be the case is provided by the detection of slowly rotating YSOs that show no evidence (from excess near- and mid-IR emission) for the presence of a circumstellar disk (Stassun et al. 1999, 2001). These observations are puzzling if one considers disk accretion to be a ubiquitous feature of star formation and interprets slow stellar rotation as due to a star-disk interaction (e.g., Königl 1991; Popham 1996). The properties of these YSOs are, however, readily understood if they are the product of a strongly braked core collapse.

## 5. SUMMARY

We study the collapse of rotating, magnetic molecular-cloud cores with the help of a self-similar model. This model generalizes the work of CCK on nonrotating cloud cores by incorporating the effects of rotation and magnetic braking (while also taking into account ambipolar diffusion and its dependence on the magnetic tension force as in the original model). We focus on the evolution after point-mass formation, noting that the pre-PMF collapse has already been studied by numerical simulations. Our approach is motivated by previous findings that simulation results for the pre-PMF collapse of rotating cores and for the pre- and post-PMF collapse of nonrotating cores are well approximated by self-similar solutions. Our semianalytic scheme allows us to examine the full range of expected behaviors and their dependence on the physical parameters. We present and analyze solutions for rotating but nonmagnetic collapsing cores, reproducing the results of Saigo & Hanawa (1998), as well as for magnetic cores in the ideal-MHD and ambipolar-diffusion limits. In these two regimes, we distinguish between fiducial solutions, obtained for typical parameter values that correspond to moderately fast initial cloud rotation rate and moderately strong magnetic braking, and limiting cases of (1) fast rotation and (2) strong braking. Our results can be summarized as follows:

- For representative parameter values, we obtain solutions that describe rotationally supported circumstellar disks of masses and sizes that are consistent with observations of YSOs. Our model thus makes it possible, for the first time, to study the formation of protostellar disks in the context of a realistic scenario of star formation in magnetically supported, weakly ionized molecular cloud cores. The outer boundary of the nearly stationary accretion disk roughly coincides with the location of the centrifugal shock, which typically occurs inward of the ambipolar-diffusion shock where the magnetic field decouples from the matter.
  - Our solutions indicate that it is quite possible that T Tauri (Class II) protostellar systems, whose disk masses are typically inferred to be  $\lesssim 10\%$  of the central mass, have had a similarly low disk-to-star mass ratio also during their earlier (Class-0 and Class-I) evolutionary phases.
  - The disk configurations that we obtain exhibit surface-density enhancements near their outer boundaries (encompassing  $\lesssim 10\%$  of the disk mass and radius for typical parameters). We speculate that these features may be the precursors of the rings detected in some Vega-like systems on scales  $\lesssim 10^2$  AU.
  - Our models allow us to elucidate the interplay between the ambipolar diffusion and magnetic braking processes. In particular, the magnetic field enhancement behind the AD shock increases the efficiency of angular-momentum removal from the disk. In the limiting case of strong braking, essentially all the angular momentum is removed well before the inflowing gas reaches the center. Such systems may correspond to slowly rotating YSOs that show no evidence of a circumstellar disk.
  - The inferred magnetic-field structures imply that the disks could drive centrifugal outflows over much of their radial extent. We show that the steady-state, radially self-similar wind solution of Blandford & Payne (1982) can be naturally incorporated into the asymptotic AD disk solution, making it possible to study the effects of wind angular-momentum and mass removal from the disk and to better constrain the relevant parameters.
  - The derived nearly-Keplerian disk configurations appear to be immune to both the magnetorotational instability and to self-gravity-induced fragmentation. Only in the limiting case of rapid initial rotation (which yields comparatively massive and largely non-Keplerian disk solutions) is the Toomre  $Q$  parameter  $< 1$  anywhere in the disk.
- Despite the various simplifications that needed to be employed to ensure self-similarity, our solutions likely capture the main qualitative aspects of the collapse of rotating cloud cores, and it is conceivable that our numerical estimates are also not too far off. Further progress in the study of protostellar disk formation could be achieved by means of numerical MHD simulations.
- We thank J. Everett, W. Herbst, Z.-Y. Li, and N. Vlahakis for helpful conversations or correspondence. We also acknowledge I. Contopoulos and G. Ciolek, whose insights on the nonrotating core-collapse problem (presented in CCK and CK) have guided us in the present work. This research was supported in part by NASA grant NAG 5-3687 and by DOE under grant B341495.

## APPENDIX

## A. DISK EQUATIONS

Assuming axisymmetry and isothermality, we write down (using cylindrical coordinates) the mass, radial momentum, and angular momentum conservation relations as well as the vertical hydrostatic equilibrium condition:

$$\frac{\partial \rho}{\partial t} + \frac{1}{r} \frac{\partial}{\partial r} (r \rho V_r) = - \frac{\partial}{\partial z} (\rho V_z), \quad (\text{A1})$$

$$\rho \frac{\partial V_r}{\partial t} + \rho V_r \frac{\partial V_r}{\partial r} = \rho g_r - C^2 \frac{\partial \rho}{\partial r} + \rho \frac{V_\phi^2}{r} + \frac{B_z}{4\pi} \frac{\partial B_r}{\partial z} - \frac{\partial}{\partial r} \left( \frac{B_z^2}{8\pi} \right) - \frac{1}{8\pi r^2} \frac{\partial}{\partial r} (r B_\phi)^2 - \rho V_z \frac{\partial V_r}{\partial z}, \quad (\text{A2})$$

$$\frac{\rho}{r} \frac{\partial}{\partial t} (r V_\phi) + \frac{\rho V_r}{r} \frac{\partial}{\partial r} (r V_\phi) = \frac{B_z}{4\pi} \frac{\partial B_\phi}{\partial z} + \frac{B_r}{4\pi r} \frac{\partial}{\partial r} (r B_\phi) - \rho V_z \frac{\partial}{\partial z} (r V_\phi), \quad (\text{A3})$$

$$C^2 \frac{\partial \rho}{\partial z} = \rho g_z - \frac{\partial}{\partial z} \left( \frac{B_\phi^2}{8\pi} + \frac{B_r^2}{8\pi} \right) + \frac{B_r}{4\pi} \frac{\partial B_z}{\partial r}, \quad (\text{A4})$$

where  $g_r$  and  $g_z$  are, respectively, the radial and vertical components of the gravitational field.

We now integrate these equations over  $z$ . We assume that the disk is geometrically thin [half-thickness  $H(r) \ll r$ ] and aim to get expressions that are valid to order  $(H/r)^2$ . On account of the disk thinness, we approximate the density, radial velocity, azimuthal velocity, and radial gravity as being constant with height. We thus equate the column density  $\Sigma \equiv \int_{-\infty}^{\infty} \rho dz$  to  $2H\rho$  and drop the last term on the right-hand side in both equations (A2) and (A3). Equation (A1) becomes

$$\frac{\partial \Sigma}{\partial t} + \frac{1}{r} \frac{\partial}{\partial r} (r \Sigma V_r) = - \frac{1}{2\pi r} \frac{\partial \dot{M}_w}{\partial r}, \quad (\text{A5})$$

where the last term on the right-hand side represents the mass flux in a disk outflow [of total outflow rate  $\dot{M}_w(r)$  within a radius  $r$ ]. We neglect this term in the calculations presented in the body of the paper, but we return in § C to consider the effect of having  $\dot{M}_w \neq 0$ .

Using the solenoidal condition on the magnetic field,  $[\partial B_z/\partial z = -r^{-1}(\partial/\partial r)(rB_r)]$ , which in a thin disk allows us to treat  $B_z$  as being constant with height whenever it is not explicitly differentiated with respect to  $z$ ] as well as the assumed field symmetry, equation (A2) integrates to

$$\begin{aligned} \Sigma \frac{\partial V_r}{\partial t} + \Sigma V_r \frac{\partial V_r}{\partial r} = \Sigma g_r - C^2 \frac{\partial \Sigma}{\partial r} + \Sigma \frac{V_\phi^2}{r} + \frac{B_z B_{r,s}}{2\pi} \\ - 2H \frac{\partial}{\partial r} \left( \frac{B_z^2}{8\pi} \right) + \frac{1}{8\pi r^2} \int_{-\infty}^{\infty} \frac{\partial}{\partial r} [r^2 (B_r^2 - B_\phi^2)] dz. \end{aligned} \quad (\text{A6})$$

Taking account of the adopted vertical mass distribution, we replace the integral in the last term of equation (A6) by an an integral over a finite interval,  $\int_{-H(r)}^{H(r)} dz$ :

$$\begin{aligned} \frac{1}{8\pi r^2} \int_{-H(r)}^{H(r)} \frac{\partial}{\partial r} [r^2 (B_r^2 - B_\phi^2)] dz = \frac{1}{8\pi r^2} \frac{\partial}{\partial r} \left[ r^2 \int_{-H(r)}^{H(r)} (B_r^2 - B_\phi^2) dz \right] \\ - \frac{1}{4\pi} (B_{r,s}^2 - B_{\phi,s}^2) \left( \frac{dH}{dr} \right) \end{aligned} \quad (\text{A7})$$

(see Lovelace, Romanova, & Newman 1994). We assume  $B_r(r, z) = B_{r,s}(r) [z/H(r)]$ , and similarly for  $B_\phi$ . This choice is motivated by the field configuration derived in the case of a rotationally supported thin disk in which the field is comparatively well coupled to the matter (e.g., Wardle & Königl 1993). Although the disks obtained in our AD collapse solutions evidently correspond to the weak-coupling case (see § 4 and Appendix C), for which this approximation is no longer adequate (e.g., Li 1996; Wardle 1997), we nevertheless adopt the above scalings for the sake of definiteness. We emphasize, however, that none of the dominant terms in the equations that we solve depends on the details of the vertical variation of these field components. We thus get

$$\begin{aligned} \frac{1}{8\pi r^2} \int_{-H(r)}^{H(r)} \frac{\partial}{\partial r} [r^2 (B_r^2 - B_\phi^2)] dz = \frac{1}{12\pi r^2} \frac{\partial}{\partial r} [r^2 H(r) (B_{r,s}^2 - B_{\phi,s}^2)] - \frac{1}{4\pi} (B_{r,s}^2 - B_{\phi,s}^2) \left( \frac{dH}{dr} \right) \\ = \frac{H}{12\pi r^2} \frac{\partial}{\partial r} [r^2 (r^2 B_{r,s}^2 - B_{\phi,s}^2)] - \frac{1}{6\pi} \left( \frac{dH}{dr} \right) (B_{r,s}^2 - B_{\phi,s}^2). \end{aligned} \quad (\text{A8})$$

Approximating  $g_r$  by  $GM(r)/r^2$  [with  $M(r) \approx M_c$  if the central mass dominates] and substituting  $J = rV_\phi$ , the integrated radial momentum equation becomes

$$\begin{aligned} \frac{\partial V_r}{\partial t} + V_r \frac{\partial V_r}{\partial r} = -\frac{GM}{r^2} - \frac{C^2}{\Sigma} \frac{\partial \Sigma}{\partial r} + \frac{J^2}{r^3} + \frac{B_z B_{r,s}}{2\pi \Sigma} - \frac{HB_z}{2\pi \Sigma} \frac{\partial B_z}{\partial r} \\ + \frac{H}{12\pi \Sigma r^2} \frac{\partial}{\partial r} (r^2 B_{r,s}^2 - r^2 B_{\phi,s}^2) - \frac{1}{6\pi \Sigma} \left( \frac{dH}{dr} \right) (B_{r,s}^2 - B_{\phi,s}^2). \end{aligned} \quad (\text{A9})$$

When integrating the angular momentum equation (A3), we write

$$\frac{B_z}{4\pi} \frac{\partial B_\phi}{\partial z} + \frac{B_r}{4\pi r} \frac{\partial}{\partial r} (rB_\phi) = \frac{1}{4\pi} \frac{\partial}{\partial z} (B_z B_\phi) + \frac{B_r}{4\pi r} \frac{\partial}{\partial r} (rB_\phi) + \frac{B_\phi}{4\pi r} \frac{\partial}{\partial r} (rB_r), \quad (\text{A10})$$

and use the same ansatz as above for  $B_r(r, z)$  and  $B_\phi(r, z)$ . We then obtain

$$\frac{\partial J}{\partial t} + V_r \frac{\partial J}{\partial r} = \frac{rB_z B_{\phi,s}}{2\pi \Sigma} + \frac{H}{6\pi r \Sigma} \frac{\partial}{\partial r} (r^2 B_{r,s} B_{\phi,s}) - \frac{rB_{r,s} B_{\phi,s}}{3\pi \Sigma} \left( \frac{dH}{dr} \right). \quad (\text{A11})$$

In integrating the vertical hydrostatic-balance equation, we take the pressure at the disk surfaces to vanish. The midplane pressure  $p_c \approx (\Sigma/2H)C^2$  is then given by

$$p_c = \frac{\pi}{2} G \Sigma^2 + \frac{GM_c \Sigma H}{4r^3} + \frac{B_{r,s}^2 + B_{\phi,s}^2}{8\pi} - \frac{HB_{r,s}}{8\pi} \frac{\partial B_z}{\partial r}, \quad (\text{A12})$$

where the first two terms on the right-hand side constitute our approximation to  $g_z$  and represent, respectively, the local disk self-gravity and the tidal squeezing by the central point mass.

The ion equation of motion is approximated by

$$\frac{\rho}{\tau_{\text{ni}}} \mathbf{V}_D = \frac{1}{4\pi} (\nabla \times \mathbf{B}) \times \mathbf{B}, \quad (\text{A13})$$

where  $\mathbf{V}_D \equiv \mathbf{V}_i - \mathbf{V}_n$ ; we assume that the disk is sufficiently weakly ionized that the neutral velocity  $\mathbf{V}_n$  is practically indistinguishable from the bulk velocity  $\mathbf{V}$ . The radial component of this equation is

$$\frac{4\pi\rho}{\tau_{\text{ni}}} V_{D,r} = B_z \left( \frac{\partial B_r}{\partial z} - \frac{\partial B_z}{\partial r} \right) - \frac{B_\phi}{r} \frac{\partial}{\partial r} (rB_\phi), \quad (\text{A14})$$

which yields, upon integration over  $z$ ,

$$V_{D,r} = \frac{\tau_{\text{ni}}}{2\pi \Sigma} B_z \left( B_{r,s} - H \frac{\partial B_z}{\partial r} \right) + \frac{\tau_{\text{ni}}}{6\pi \Sigma} \left[ \frac{H}{r} \left( B_{r,s} \frac{\partial B_{r,s}}{\partial r} - B_{\phi,s} \frac{\partial B_{\phi,s}}{\partial r} \right) + (B_{\phi,s}^2 - B_{r,s}^2) \left( \frac{dH}{dr} \right) \right] \quad (\text{A15})$$

(see eq. [A9]). Similarly, the azimuthal component of equation (A13),

$$\frac{4\pi\rho}{\tau_{\text{ni}}}V_{D,\phi} = B_z \frac{\partial B_\phi}{\partial z} + \frac{B_r}{r} \frac{\partial}{\partial r} (rB_\phi), \quad (\text{A16})$$

gives, when integrated over  $z$ ,

$$V_{i,\phi} = V_\phi + \frac{\tau_{\text{ni}}}{2\pi\Sigma} B_z B_{\phi,s} + \frac{\tau_{\text{ni}} H}{6\pi\Sigma r} \frac{\partial}{\partial r} (r^2 B_{r,s} B_{\phi,s}) - \frac{\tau_{\text{ni}}}{3\pi\Sigma} B_{r,s} B_{\phi,s} r \left( \frac{dH}{dr} \right) \quad (\text{A17})$$

(see eq. [A11]).

The flux conservation equation is obtained from Faraday's law ( $\partial \mathbf{B} / \partial t = -c \nabla \times \mathbf{E}$ ) and Ohm's law in the ambipolar diffusion-dominated regime ( $c\mathbf{E} = -\mathbf{V}_i \times \mathbf{B}$ ) together with equation (A13). The result is

$$\frac{\partial \mathbf{B}}{\partial t} = \nabla \times (\mathbf{V} \times \mathbf{B}) + \nabla \times \left\{ \frac{\tau_{\text{ni}}}{4\pi\rho} [(\nabla \times \mathbf{B}) \times \mathbf{B}] \times \mathbf{B} \right\}. \quad (\text{A18})$$

The  $z$  component of this equation is

$$\begin{aligned} \frac{\partial B_z}{\partial t} &= \frac{1}{2\pi r} \frac{\partial}{\partial r} \left( \frac{\partial \Psi}{\partial t} \right) \\ &= \frac{1}{r} \frac{\partial}{\partial r} \left( -rV_r B_z + \frac{\tau_{\text{ni}} r}{4\pi\rho} \left\{ -B_z \left[ B_z \left( \frac{\partial B_r}{\partial z} - \frac{\partial B_z}{\partial r} \right) - \frac{B_\phi}{r} \frac{\partial}{\partial r} (rB_\phi) \right] \right. \right. \\ &\quad \left. \left. - B_r \left[ B_\phi \frac{\partial B_\phi}{\partial z} + B_r \left( \frac{\partial B_r}{\partial z} - \frac{\partial B_z}{\partial r} \right) \right] \right\} \right), \end{aligned} \quad (\text{A19})$$

which implies

$$\frac{2}{r} \frac{\rho}{\tau_{\text{ni}}} \left( \frac{\partial \Psi}{\partial t} + 2\pi r V_r B_z \right) = -(B_z^2 + B_r^2) \left( \frac{\partial B_r}{\partial z} - \frac{\partial B_z}{\partial r} \right) + \frac{B_\phi B_z}{r} \frac{\partial}{\partial r} (rB_\phi) - B_r B_\phi \frac{\partial B_\phi}{\partial z}. \quad (\text{A20})$$

Integrating this over  $z$  and rearranging, gives

$$\begin{aligned} \frac{\partial \Psi}{\partial t} &= -2\pi r V_r B_z + \frac{r\tau_{\text{ni}}}{\Sigma} \left\{ - \left( B_{r,s} - H \frac{\partial B_z}{\partial r} \right) \left( B_z^2 + \frac{1}{3} B_{r,s}^2 \right) \right. \\ &\quad \left. + \frac{1}{3} B_{\phi,s}^2 \left[ -B_{r,s} + H B_z \left( \frac{d}{dr} \ln(rB_{\phi,s}) - \frac{d \ln H}{dr} \right) \right] \right. \\ &\quad \left. - \frac{1}{3} B_{r,s}^2 \left[ H B_z \left( \frac{d}{dr} \ln(rB_{r,s}) - \frac{d \ln H}{dr} \right) \right] \right\}. \end{aligned} \quad (\text{A21})$$

In formulating the self-similar model in § 2.2 we use a pared-down version of the above equations. This is motivated by our finding that our basic results can be derived *without* including any  $\mathcal{O}(H/r)$  terms. The only instance in which a term of this order plays a role in our solutions is in allowing us to refine the structure of the ambipolar-diffusion shock by employing the radial gradient of  $B_z$  in the radial momentum equation. We therefore retain the combination  $[B_{r,s} - H(\partial B_z / \partial r)]$  (which is proportional to the vertically integrated azimuthal component of the current density) in equation (A9) but neglect the other two  $\mathcal{O}(H/r)$  terms in that equation, since they typically do not exceed the  $\propto \partial B_z / \partial r$  term. [The last two terms in equation (A9) can become much larger than the  $\propto \partial B_z / \partial r$  term in the limit  $r/t \rightarrow 0$  of the IMHD solution, when  $B_{r,s}/B_z$  formally diverges. However, as we argue in § 3, this divergence is not expected to occur in a real disk. Furthermore, the neglect of these terms is justified even in our formal solution since  $H \propto 1/B_{r,s}^2$  in this limit, so the radial derivative terms remain negligible in comparison with the magnetic tension ( $\propto B_z B_{r,s}$ ) term.] Since the same integrated current density component appears also in equations (A15) and (A21) for  $V_{D,r}$  and  $\partial \Psi / \partial t$ , respectively, we keep the combination  $[B_{r,s} - H(\partial B_z / \partial r)]$  in these equations too for self-consistency, but we again omit all the other  $\mathcal{O}(H/r)$  terms. For the same reason we keep the  $\propto H(\partial B_z / \partial r)$  term also in the vertical force balance equation (A12), which means that we end up retaining all the  $\mathcal{O}(H/r)$  terms in this ‘‘master equation’’ for  $H$ .

We similarly neglect the  $\mathcal{O}(H/r)$  terms in the angular momentum equation (A11) and, correspondingly, in equation (A17) for  $V_{i,\phi}$ . The latter equation can then be substituted into equation (3) to yield a purely algebraic expression for  $B_{\phi,s}$ .

## B. SINGULAR LINES AND SHOCK JUMP CONDITIONS

The singular lines of the flows considered in this paper can be obtained by rewriting the radial momentum equation (21) in the form

$$(1 - w^2) \frac{d\sigma}{dx} = -b_z h \frac{db_z}{dx} + [\dots]. \quad (\text{B1})$$

In the AD limit, in which the field is effectively decoupled from the bulk of the matter, we immediately infer that the singular line corresponds to the sonic speed:

$$(x - u)^2 = 1 \quad (\text{AD limit}) \quad (\text{B2})$$

(see CCK for a discussion of the physical basis of this result).

In the ideal-MHD limit, flux freezing implies  $b_z / \sigma = 1 / \mu_0$  (see eq. [33]), and therefore the singular line is given by

$$(x - u)^2 = 1 + h\sigma / \mu_0^2 \quad (\text{IMHD limit}). \quad (\text{B3})$$

In the region where self-gravity dominates,  $h \approx 2/\sigma$ , and equation (B3) reduces to  $(x - u)^2 = 1 + 2/\mu_0^2$ , which is the result given by equation (41) in CCK.<sup>5</sup> In dimensional form, equation (B3) is

$$(r/t - V_r)^2 = C^2 + B_z^2 H / 2\pi \Sigma = C^2 + B_z^2 / 4\pi \rho, \quad (\text{B4})$$

where the last term on the right-hand side is equal to the Alfvén speed in the disk. The IMHD singular line thus corresponds to the fast-magnetosonic speed, which agrees with (and generalizes) the statement made in CCK on the basis of the self-gravity-dominated limit of equation (B3).

When the curve describing the flow crosses and falls below the singular line in the  $\{x, u\}$  plane, this generally signals the appearance of an unresolved shock discontinuity. In the present work, this is the situation invariably encountered in the vicinity of the centrifugal radius. To properly model this discontinuity, appropriate shock jump conditions need to be applied. The conservation of mass across the shock yields

$$\sigma w_s = \text{const}, \quad (\text{B5})$$

where  $w_s \equiv x_s - u$  (with  $x_s$  denoting the shock location). When the ions and neutrals are well coupled inside the shock, the magnetic-flux conservation condition takes the form

$$b_z w_s = \text{const}. \quad (\text{B6})$$

In the strong-coupling case, equations (B5) and (B6) imply  $\mu \equiv \sigma/b_z = \text{const}$  across the shock: in what follows we set  $\mu = \mu_0$ , which applies when the entire flow upstream of the shock obeys ideal MHD. Under the adopted isothermal approximation, the jump conditions are fully specified once we integrate also the differential terms in equation (B1) across the discontinuity. Performing this integral requires making some assumptions about the behavior of  $\sigma$ ,  $b_z$ , and  $h$  in the shock region. In the following subsections, we consider four cases in which algebraic jump conditions can be derived. These results have enabled us to explicitly model the centrifugal shock in all the core-collapse solutions presented in this paper.

### B.1. Isothermal Shock

If one can neglect variations in the magnetic field across the discontinuity, as is the case when the centrifugal shock occurs deep inside the AD regime (see § 3.3.1), equations (B1) and (B5) imply

$$\sigma(w_s^2 + 1) = \text{const}. \quad (\text{B7})$$

Denoting the upstream and downstream sides of the shock by the subscripts 1 and 2, respectively, one can use equations (B7) and (B5) to express the nontrivial ( $w_{s1} \neq w_{s2}$ ) solution in the form  $w_{s1} w_{s2} = 1$ . This is the simplest realization of the “isothermal” jump conditions discussed by Shu & Li (1997).

### B.2. Generalized Isothermal Shock

If the shock occurs in the self-gravitating regime, where  $h \approx 2/\sigma$ , then  $b_z h \propto b_z/\sigma$  is constant across the shock, and the integration of equation (B1) leads to

$$\sigma(w_s^2 + \Theta) = \text{const}, \quad (\text{B8})$$

where  $\Theta \equiv 1 + 2/\mu_0^2$ . This situation is encountered in the fast-rotation solutions presented in § 3.2.2 and § 3.3.2. In this case the upstream and downstream radial velocities (in the shock frame) are related by  $w_{s1} w_{s2} = \Theta$ , which constitutes another realization of the “isothermal” jump conditions. remark. [Note that, as  $w_{s2} \rightarrow w_{s1}$ , one recovers the singular-line relation (eq. [B3]) for a self-gravitating IMHD flow.]

### B.3. Magnetically Squeezed Shock

If magnetic squeezing due to the radial field dominates gravity in the vertical force-balance equation, then  $h \approx 2\sigma b_{r,s}^{-2}$  (see eq. [42]), and equation (B1) yields

$$\sigma(w_s^2 + 1) + \frac{2\sigma^3}{3\mu_0^2 b_{r,s}^2} = \text{const}. \quad (\text{B9})$$

Taking into account the relation (B5), we obtain a quartic equation for  $\sigma_2$  (whose coefficients are combinations of the upstream flow variables). We can eliminate the trivial solution  $\sigma_2 = \sigma_1$  by dividing this equation by  $(\sigma_2 - \sigma_1)$ , which reduces it to

$$\sigma_2^3 + \sigma_1 \sigma_2^2 + (\sigma_1^2 + Q) \sigma_2 - \sigma_1 (u_1 - x_s)^2 Q = 0, \quad (\text{B10})$$

where  $Q \equiv 3\mu_0^2 b_{r,s}^2 / 2$ . Equation (B10) is a cubic of the form  $\sigma_2^3 + a_2 \sigma_2^2 + a_1 \sigma_2 + a_0 = 0$ , whose discriminant is  $D = (p/3)^3 + (q/2)^2$ , with  $p = a_1 - a_2^2/3$  and  $q = a_0 - a_1 a_2/3 + 2a_2^3/27$ . For this particular cubic, the discriminant is always positive, guaranteeing that there is exactly one real root, given by

$$\sigma_2 = -a_2/3 + q_+ + q_-, \quad (\text{B11})$$

where  $q_{\pm} \equiv (-q/2 \pm \sqrt{D})^{1/3}$ . This solution provides a good approximation to the centrifugal shock in the fiducial IMHD flow (§ 3.2.1).

<sup>5</sup> Equation (41) in CCK is therefore only a special case of the more general expression, which is given by equation (B3).

#### B.4. Constant-Thickness Shock

Another possibility is that  $h$  is constant across the shock, as would be the case if the central point-mass gravity controlled the squeezing in the vertical equilibrium equation (see eqs. [57] and [71]). In this case, integration of equation (B1) results in

$$\sigma(w^2 + 1) + b_z^2 h/2 = \text{const.} \quad (\text{B12})$$

In conjunction with the mass conservation equation (B5), this can be written as a cubic equation for  $\sigma_2$ . After factoring out the trivial solution, one obtains a quadratic equation,

$$\sigma_2^2 + (\sigma_1 + 2\mu_0/h)\sigma_2 - (m/x_s)^2(2\mu_0/h\sigma_1) = 0, \quad (\text{B13})$$

which has exactly one positive real root. In order for this result to be applicable to a centrifugal shock in a collapsing magnetized core, the shock must occur far enough from the center that ideal MHD is still a good approximation (so that the magnetic term in eq. [B1] continues to play a role). However, in the solutions explored in this paper, the requirements that the central gravity dominate the vertical squeezing and that the IMHD regime be applicable are never satisfied at the location of the centrifugal shock: in the fiducial and strong-gravity IMHD cases, magnetic squeezing exceeds the tidal force in the central gravity-dominated region, whereas in the fast-rotation IMHD and AD cases, self-gravity dominates at the location of the shock.

### C. INCORPORATION OF A CENTRIFUGALLY DRIVEN WIND INTO THE DISK SOLUTION

As we note in § 4, the asymptotic ambipolar-diffusion disk solution satisfies the launching condition  $B_{r,s}/B_z > 1/\sqrt{3}$  for a cold, centrifugally driven wind, and, in fact, implies a radial scaling of the magnetic field components (at any given instant of time) that is identical to that of the time-independent, radially self-similar wind solution of Blandford & Payne (1982, hereafter BP). Once a super-Alfvénic wind of this type is established, it constitutes the dominant mechanism of removing angular momentum from the disk (at least in the vertical direction). Furthermore, if the outflow is quasi steady on the accretion time scale, then the spatially self-similar wind solution can be used to determine the value of  $B_{\phi,s}$  (or, equivalently, of the parameter  $\delta$ ) in the asymptotic self-similar (in space and time) disk solution. An explicit wind solution also makes it possible to evaluate the reduction in the mass accretion rate onto the central star caused by the diversion of part of the inflowing mass into a disk outflow. Motivated by these considerations, we now show how the centrifugally driven wind solution can be incorporated into the asymptotic AD disk model. As demonstrated in § 3.3.1, the numerical solution of the disk equations typically converges rapidly behind the centrifugal shock to the asymptotic form given by equations (51)–(57). This indicates that, if the model parameters do not strongly differ from the fiducial values, then the results that we obtain for the asymptotic regime should be applicable to the bulk of the rotationally supported disk that forms around the central object.

The mass loss in the BP model is constant for each decade of disk radius and can be related to the accretion rate  $\dot{M}_c$  at the inner edge of the disk by

$$\frac{1}{2\pi r} \frac{\partial \dot{M}_w}{\partial r} = \frac{\epsilon \dot{M}_c}{2\lambda - 3} \frac{1}{2\pi r^2}, \quad (\text{C1})$$

where  $\epsilon \leq 1$  is the fraction of the disk binding energy at its inner edge  $r_{\text{in}}$  that is carried off by the wind, and where  $\lambda$  is the total (kinetic plus magnetic) specific angular momentum in the wind, normalized by the Keplerian disk value  $rV_K = (GM_c r)^{1/2}$ . The field-line constant  $\lambda$  is one of the three parameters that define a solution in the cold, self-similar BP wind model, the other two being  $\xi'_0 \equiv B_{r,s}/B_z$  and  $\kappa \equiv 4\pi\rho V_z V_K/B_z^2$  (the normalized mass-to-magnetic flux ratio evaluated at the disk surface). As we noted above, for any given value of  $t$  in the asymptotic AD disk solution,  $B_{r,s}/B_z$  is a spatial constant ( $= 4/3$ ; see eq. [56]) that exceeds the launching threshold  $1/\sqrt{3}$ . It is thus natural to set  $\xi'_0 = 4/3$ . One can then evaluate the parameter  $\kappa$  by equating  $2\rho V_z$  with the expression given by equation (C1) (where the factor of 2 accounts for the two disk surfaces). The result (in terms of the nondimensional flow quantities introduced in § 2.3) is

$$\kappa = \frac{\epsilon \dot{m}_c m_c^{1/2}}{(2\lambda - 3)b_z^2 x^{5/2}}. \quad (\text{C2})$$

Substituting for  $m_c$  and  $b_z$  from the asymptotic-solution equations (51) and (55), respectively, this becomes

$$\kappa = \frac{2\delta\epsilon}{2\lambda - 3}. \quad (\text{C3})$$

We now substitute for  $\delta$  in the asymptotic disk solution the corresponding expression in the BP wind model,

$$\delta = -\frac{b_{\phi,s}}{b_z} = \kappa(\lambda - 1), \quad (\text{C4})$$

which yields

$$\lambda = \frac{3 - 2\epsilon}{2(1 - \epsilon)}. \quad (\text{C5})$$

Although we started by evaluating  $\kappa$ , we ended up with an expression that gives  $\lambda$  in terms of  $\epsilon$ . The latter parameter was treated by BP as being distinct from  $\lambda$ , but we are now able to relate them by combining the disk and wind solutions. By fixing the values of  $\xi'_0$  and  $\lambda$ , one can derive the value of  $\kappa$  from the solution of the self-similar wind equations (see Fig. 2 in BP), and thereby obtain  $\delta$  (using eq. [C4]). In practice, this “recipe” for incorporating the wind model does not alter our basic disk model since it effectively amounts to replacing one somewhat arbitrary parameter ( $\delta$ ) by another ( $\epsilon$ ). However, by combining the disk and wind solutions, it is

possible to constrain the parameter values. In particular, by requiring that the flow be magnetically dominated in the vicinity of the disk (which implies  $\kappa < 1$ ) and that it become super-Alfvénic at a finite height, one can infer a lower bound on  $\lambda$ . Based on Figure 2 in BP, this lower limit is  $\sim 3$  for  $\xi_0^t = 4/3$  (which, by eq. [C5], implies that  $\epsilon$  must be  $\gtrsim 0.75$ ), and as  $\lambda$  increases from  $\sim 3$  to  $\sim 30$  (corresponding to  $\epsilon$  increasing from  $\sim 0.75$  to  $\sim 0.98$ ),  $\delta$  decreases from  $\sim 2$  to  $\sim 0.3$ .

In the absence of a disk outflow, the central mass eigenvalue  $m_c$  is given approximately by the product  $-xu\sigma$  evaluated at  $x_c$  (see eqs. [26] and [51]). When the mass loss between the outer edge of the disk ( $r_{\text{out}} \approx r_c$ ) and its inner edge ( $r_{\text{in}} \approx R_*$ , the protostellar radius) is taken into account in the mass conservation equation, the value of  $m_c$  is reduced to

$$m_c \approx \left[ 1 + \frac{\ln \Lambda}{2(\lambda - 1)} \right]^{-1} (-xu\sigma)_{x_c}, \quad (\text{C6})$$

where  $\Lambda \equiv r_{\text{out}}/r_{\text{in}}$  (see eqs. [A5], [C1], and [C5]). To the extent that deuterium burning causes the radius of the accreting protostar to increase roughly linearly with its mass (e.g., Stahler 1988),  $\Lambda$  can be approximated as a constant. Estimating  $r_c$  from our fiducial AD solution (see eq. [65]) and  $R_*$  from the mass–radius relation given by Stahler (1988), we obtain  $\ln \Lambda \approx 8$ . Equation (C6) then implies that mass outflow from the disk surfaces could reduce the accretion rate onto the central object by a factor as large as  $\sim 3$  (using the minimum value of  $\lambda$ , which corresponds to  $\kappa = 1$ ). More strongly magnetized outflows have lower  $m_c$  reduction factors: for example, when  $\kappa$  decreases to  $\lesssim 0.1$  (corresponding to  $\lambda \gtrsim 10$  and  $\delta \lesssim 1$ ), this factor declines to  $\lesssim 1.5$ . Although the cumulative effect of the mass loss from the wind surfaces (embodied in the factor  $\ln \Lambda$ ) can be significant, its impact at any given radius is comparatively small because of the large range of radii involved ( $r_{\text{out}}/r_{\text{in}} \approx 3 \times 10^3$  in the fiducial case). The incorporation of a disk wind modifies the integrated self-similar disk equations only through logarithmic terms in  $x$ , so to lowest order the power-law scalings of the asymptotic disk solution remain unchanged.

Explicit models of AD-dominated, wind-driving accretion disks were previously constructed by Wardle & Königl (1993) and Li (1996). Two general types of solutions were obtained, depending on the value of the neutral–ion coupling parameter  $\eta_{\text{WKL}} \equiv 1/\tau_{\text{ni}}\Omega_K$ . Strongly coupled disks have  $\eta_{\text{WKL}} \gtrsim 1$  at all heights and are characterized by the thermal pressure not being much larger than the magnetic pressure at  $z = 0$ , by  $B_r$  starting to increase already near the midplane and generally exceeding  $|B_\phi|$  at the disk surface (which leads to a strong magnetic squeezing of the disk), and by the inflow speed typically being  $\gtrsim C$  (Wardle & Königl 1993). In contrast, in weakly coupled disks (characterized by  $\eta_{\text{WKL}} < 1$  over the bulk of the vertical column) the thermal pressure can be much larger than the magnetic pressure at  $z = 0$ ,  $B_r$  only starts to grow well above the midplane (at a height where the coupling parameter finally rises above 1) and usually does not exceed  $|B_\phi|$  at the surface (which results in the magnetic squeezing remaining relatively unimportant), and the mass-averaged inflow speed is typically well below  $C$  (Li 1996). As we point out in § 4,  $\eta_{\text{WKL}}$  is equal to  $2/3\delta$  in the asymptotic AD disk solution. This result is compatible with the just-described behavior of  $B_{r,s}$  and  $|B_{\phi,s}|$ : since  $B_{r,s}/B_z = 4/3$  in the asymptotic solution and  $\delta = |B_{\phi,s}|/B_z$ , the expression for  $\eta_{\text{WKL}}$  implies  $B_{r,s}/|B_{\phi,s}| = 2\eta_{\text{WKL}}$  [consistent with eq. (4.5) in Wardle & Königl (1993) and eq. (39) in Li (1996)]. The values of  $\delta$  derived from the BP wind solution indicate that our AD disks are likely to be weakly coupled. This conclusion is consistent with the low magnetic-to-thermal pressure ratio implied by the asymptotic disk solution (it is  $\propto r^{1/2}$  as  $r \rightarrow 0$  at any given instant of time; see eqs. [54]–[57]), which corresponds to the situation in weakly coupled disks. The association with the weakly coupled class of solutions is further indicated by the unimportance of magnetic squeezing in the asymptotic expression for the disk half-thickness (eq. [57]) and by the subsonic inflow speed inferred in the asymptotic regime ( $V_r/C \propto r^{1/2}$  as  $r \rightarrow 0$  and  $t$  is held fixed; see eq. [53]). The inner regions of real protostellar disks (on radial scales  $\sim 0.1$ – $10$  AU) are, in fact, expected to be so weakly ionized over most of their interiors that the requisite field-line bending for launching a centrifugal wind can only occur in comparatively thin surface layers (e.g., Wardle 1997). As was, however, already emphasized by Li (1996), the properties of such disks and of their associated outflows depend sensitively on the details of the spatial profile of  $\eta_{\text{WKL}}$ . Further progress in developing these models will thus require a good understanding of the ionization structure in the inner regions of protostellar disks.

## REFERENCES

- Balbus, S. A., & Hawley, J. F. 1998, *Rev. Mod. Phys.*, 70, 1  
 Basu, S. 1997, *ApJ*, 485, 240  
 Basu, S. 1998, *ApJ*, 509, 229  
 Basu, S., & Mouschovias, T. Ch. 1994, *ApJ*, 432, 720  
 Basu, S., & Mouschovias, T. Ch. 1995a, *ApJ*, 452, 386  
 Basu, S., & Mouschovias, T. Ch. 1995b, *ApJ*, 453, 271  
 Beckwith, S. V. W., & Sargent, A. I. 1993, in *Protostars and Planets III*, ed. E. H. Levy & J. I. Lunine (Tucson: University of Arizona Press), 521  
 Blaes, O. M., & Balbus, S. A. 1994, *ApJ*, 421, 163  
 Blandford, R. D., & Payne, D. G. 1982, *MNRAS*, 199, 883 (BP)  
 Bodenheimer, P., Burkert, A., Klein, R. I., & Boss, A. P. 2000, in *Protostars and Planets IV*, ed. V. Mannings, A. P. Boss, & S. S. Russell (Tucson: University of Arizona Press), 675  
 Boss, A. P. 2000, *ApJ*, 545, L61  
 Calvet, N., Hartmann, L., & Strom, S. E. 2000, in *Protostars and Planets IV*, ed. V. Mannings, A. P. Boss, & S. S. Russell (Tucson: University of Arizona Press), 377  
 Cassen, P. M., & Summers, A. L. 1983, *Icarus*, 53, 26  
 Ciolek, G. E., & Königl, A. 1998, *ApJ*, 504, 257 (CK)  
 Ciolek, G. E., & Mouschovias, T. Ch. 1998, *ApJ*, 504, 280  
 Contopoulos, I., Ciolek, G. E., & Königl, A. 1998, *ApJ*, 504, 247 (CCK)  
 Contopoulos, I., & Sauty, C. 2001, *A&A*, 365, 165  
 Crutcher, R. M. 1999, *ApJ*, 520, 706  
 D’Alessio, P., Canto, J., Calvet, N., & Lizano, S. 1998, *ApJ*, 500, 411  
 Dent, W. R. F., Walker, H. J., Holland, W. S., & Greaves, J. S. 2000, *MNRAS*, 314, 702  
 Desch, S. J., & Mouschovias, T. Ch. 2001, *ApJ*, 550, 314  
 Dutrey, A., Guilloteau, S., Prato, L., Simon, M., Duvert, G., Schuster, K., & Menard, F. 1998, *A&A*, 338, L63  
 Fiedler, R. A., & Mouschovias, T. Ch. 1993, *ApJ*, 415, 680  
 Galli, D., & Shu, F. H. 1993, *ApJ*, 417, 243  
 Goodman, A. A., Benson, P. J., Fuller, G. A., & Myers, P. C. 1993, *ApJ*, 406, 528  
 Goodson, A. P., & Winglee, R. M. 1999, *ApJ*, 524, 159  
 Guilloteau, S., & Dutrey, A. 1998, *A&A*, 339, 467  
 Hartmann, L., Calvet, N., Gullbring, E., & D’Alessio, P. 1998, *ApJ*, 495, 385  
 Hawley, J. F., & Stone, J. M. 1998, *ApJ*, 501, 758  
 Hayashi, C., Nakazawa, K., & Nakagawa, Y. 1985, in *Protostars & Planets II*, ed. D. C. Black & M. S. Mathews (Tucson: University of Arizona Press), 1100  
 Indebetouw, R., & Zweibel, E. G. 2000, *ApJ*, 532, 361  
 Kamaya, H., & Nishi, R. 2000, *ApJ*, 543, 257  
 Kane, B. D., & Clemens, D. P. 1997, *AJ*, 113, 1799  
 Koerner, D. W., Sargent, A. I., & Ostroff, N. A. 2001, *ApJ*, 560, L181  
 Königl, A. 1987, *ApJ*, 320, 726  
 Königl, A. 1991, *ApJ*, 370, L79



- Königl, A., & Pudritz, R. E. 2000, in *Protostars and Planets IV*, ed. V. Mannings, A. P. Boss, & S. S. Russell (Tucson: University of Arizona Press), 759
- Li, Z.-Y. 1996, *ApJ*, 465, 855
- Li, Z.-Y. 1998, *ApJ*, 497, 850
- Li, Z.-Y., & McKee, C. F. 1996, *ApJ*, 464, 373
- Li, Z.-Y., & Shu, F. H. 1997, *ApJ*, 475, 237
- Lin, D. N. C., & Pringle, J. E. 1987, *MNRAS*, 225, 607
- Lin, D. N. C., & Pringle, J. E. 1990, *ApJ*, 358, 515
- Lovelace, R. V. E., Romanova, M. M., & Newman, W. I. 1994, *ApJ*, 437, 136
- Matsumoto, T., Hanawa, T., & Nakamura, F. 1997, *ApJ*, 478, 569
- Mestel, L., & Spruit, H. C. 1987, *MNRAS*, 226, 57
- Mineshige, S., & Umemura M. 1997, *ApJ*, 480, 167
- Mouschovias, T. Ch., & Ciolek, G. E. 1999, in *The Origins of Stars and Planetary Systems*, ed. C. J. Lada & N. D. Kylafis (Dordrecht: Kluwer), 305
- Mouschovias, T. Ch., & Paleologou, E. V. 1986, *ApJ*, 308, 781
- Mundy, L. G., Looney, L. W., & Welch, W. J. 2000, in *Protostars and Planets IV*, ed. V. Mannings, A. P. Boss, & S. S. Russell (Tucson: University of Arizona Press), 355
- Myers, P. C., Evans, N. J., & Ohashi, N. 2000, in *Protostars and Planets IV*, ed. V. Mannings, A. P. Boss, & S. S. Russell (Tucson: University of Arizona Press), 217
- Nakamura, F., Hanawa, T., & Nakano, T. 1995, *ApJ*, 444, 770
- Nakamura, F., Matsumoto, T., Hanawa, T., & Tomisaka, K. 1999, *ApJ*, 510, 274
- Narita, S., Hayashi, C., & Miyama, S. M. 1984, *Prog. Theor. Phys.*, 72, 1118
- Neufeld, D. A., & Hollenbach, D. J. 1994, *ApJ*, 428, 170
- Nishi, R., Nakano, T., & Umebayashi, T. 1991, *ApJ*, 368, 181
- Norman, M. L., Wilson, J. R., & Barton, R. T. 1980, *ApJ*, 239, 968
- Ohashi, N., Hayashi, M., Ho, P. T. P., Momose, M., Tamura, M., Hirano, N., & Sargent, A. I. 1997, *ApJ*, 488, 317
- Popham, R. 1996, *ApJ*, 467, 749
- Saigo, K., & Hanawa, T. 1998, *ApJ*, 493, 342
- Schneider, G., et al. 1999, *ApJ*, 513, L127
- Shakura, N. I., & Sunyaev, R. A. 1973, *A&A*, 24, 337
- Shu, F. H., & Li, Z.-Y. 1997, *ApJ*, 475, 251
- Stahler, S. W. 1988, *ApJ*, 332, 804
- Stassun, K. G., Mathieu, R. D., Mazeh, T., & Vrba, F. J. 1999, *AJ*, 117, 2941
- Stassun, K. G., Mathieu, R. D., Vrba, F. J., Mazeh, T., & Henden, A. 2001, *AJ*, 121, 1003
- Terebey, S., Shu, F. H., & Cassen, P. 1984, *ApJ*, 286, 529
- Tomisaka, K. 1996, *PASJ*, 48, 701
- Tomisaka, K. 1998, *ApJ*, 502, L163
- Tomisaka, K. 2000, *ApJ*, 528, L41
- Tomisaka, K. 2002, *ApJ*, 575, 306
- Toomre, A. 1964, *ApJ*, 139, 1217
- Tsuribe, T. 1999, *ApJ*, 527, 102
- Wardle, M. 1997, in *ASP Conf. Ser. 121, Accretion Phenomena and Related Outflows*, ed. D. T. Wickramasinghe, G. V. Bicknell, & L. Ferrario (San Francisco: ASP), 561
- Wardle, M., & Königl, A. 1993, *ApJ*, 410, 218
- Wardle, M., & Ng, C. 1999, *MNRAS*, 303, 239
- Weidenschilling, S. J. 1977, *Ap&SS*, 51, 153
- Wilner, D. J., & Lay, O. P. 2000, in *Protostars and Planets IV*, ed. V. Mannings, A. P. Boss, & S. S. Russell (Tucson: University of Arizona Press), 509
- Wuchterl, G., Guillot, T., & Lissauer, J. J. 2000, in *Protostars and Planets IV*, ed. V. Mannings, A. P. Boss, & S. S. Russell (Tucson: University of Arizona Press), 1081
- Yorke, H. W., Bodenheimer, P., & Laughlin, G. 1993, *ApJ*, 411, 274
- Zweibel, E. G. 1998, *ApJ*, 499, 746